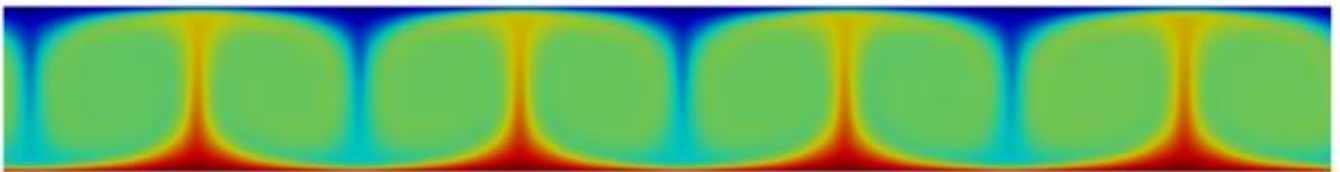


Algebraic heat flux modeling for  
numerical prediction of heat trans-  
fer and flow in Natural Convection  
MSc Thesis

Kunal Kanawade

Technische Universiteit Delft





# Algebraic heat flux modeling for numerical prediction of heat transfer and flow in Natural Convection

MSC THESIS

by

**Kunal Kanawade**

in partial fulfillment of the requirements for the degree of

**Master of Science**  
in Aerospace Engineering

at the Delft University of Technology,  
to be defended publicly on Thursday December 19, 2019 at 9:30 AM.

Supervisors:	Dr. ir. A. Shams,	Nuclear Research and Consultancy Group, Petten
	Dr. ir. M. I. Gerritsma,	Aerodynamics, LR Faculty, TU Delft
Readers:	Dr. ir. A. H. van Zuijlen,	Aerodynamics, LR Faculty, TU Delft
	Ir. J. Sinke,	Aerospace Structures and Materials, LR Faculty, TU Delft
	Dr. ir. G. A. Bohlin,	Flight Propulsion and Power, LR Faculty, TU Delft

*This thesis is confidential and cannot be made public until December 31, 2024.*

An electronic version of this thesis is available at <http://repository.tudelft.nl/>.



# LIST OF FIGURES

2.1	Conservation in a discrete element . . . . .	8
2.2	Varying integration points for source integrals . . . . .	10
4.1	Evolution of mean temperature profile for $Re_\tau = 395$ at (Left) $Pr=1$ and (Right) $Pr=0.025$ . . . . .	19
4.2	Models for $Pr_t$ number compared to the LES for $Re_\tau = 590$ at (Left) $Pr=0.01$ (.) and (Right) $Pr=0.025$ (o): Reynolds [1]( <i>dash-dot</i> ), Kays [2]( <i>dash</i> ) and Weigand et al. [3]( <i>solid</i> ) [4]. . . . .	20
4.3	Temperature profiles of RANS at $Re = 2000$ LES (black solid), linear law and $Pr_t = 0.85$ (green), linear law $\theta^+ = Pr \cdot y^+$ (black dashed), wall-resolved RANS with Kays correlation (blue), mixed law-of-the-wall and Kays (red). [5]. . . . .	21
4.4	Graphical representation of $C_{t_3}$ for AHFM-NRG: $k-\epsilon$ and AFHM-NRG+: $RSM-EB$ . . . . .	24
5.1	Computational domain for the RBC case . . . . .	26
5.2	Velocity Contour for Ra 630000 Pr 0.7 . . . . .	27
5.3	Temperature Contour for Ra 630000 Pr 0.7 . . . . .	27
5.4	DNS case geometry with boundary conditions imposed . . . . .	29
5.5	Mean temperature distribution for Ra 2e7 Pr 0.7 . . . . .	30
5.6	Temperature Variance for Ra 2e7 Pr 0.7 . . . . .	31
5.7	Mean temperature distribution for Ra 630000 Pr 0.7 . . . . .	32
5.8	Temperature Variance for Ra 630000 Pr 0.7 . . . . .	33
5.9	Turbulent kinetic energy for Ra 630000 Pr 0.7 . . . . .	33
5.10	Turbulent heat fluxes for Ra 630000 Pr 0.7 . . . . .	34
5.11	Mean temperature distribution for Ra 381e3 Pr 0.7 . . . . .	35
5.12	Temperature Variance for Ra 381e3 Pr 0.7 . . . . .	36
5.13	Turbulent kinetic energy for Ra 381e3 Pr 0.7 . . . . .	36
5.14	Mean temperature distribution for Ra 1e5 Pr 0.025 . . . . .	37
5.15	Temperature Variance for Ra 1e5 Pr 0.025 . . . . .	38
5.16	Turbulent kinetic energy for Ra 1e5 Pr 0.025 . . . . .	38
5.17	Turbulent heat fluxes for Ra 1e5 Pr 0.025 . . . . .	39
5.18	Mean temperature distribution for Ra 5e4 Pr 0.025 . . . . .	40
5.19	Temperature Variance for Ra 5e4 Pr 0.025 . . . . .	40
5.20	Turbulent kinetic energy for Ra 5e4 Pr 0.025 . . . . .	41
5.21	Mean temperature distribution for Ra 24e3 Pr 0.006 . . . . .	42
5.22	Temperature Variance for Ra 24e3 Pr 0.006 . . . . .	42
5.23	Turbulent kinetic energy for Ra 24e3 Pr 0.006 . . . . .	43
5.24	Turbulent heat fluxes for Ra 24e3 Pr 0.006 . . . . .	43
A.1	Mean temperature distribution for considered three meshes . . . . .	48
A.2	Turbulent Kinetic Energy distribution for considered three meshes . . . . .	48
A.3	Temperature variance distribution for considered three meshes . . . . .	49
A.4	Perturbations in Temperature profile . . . . .	50



# LIST OF TABLES

3.1	Model coefficients for RSM-EB formulation [6]	16
5.1	Summary for boundary conditions imposed in the domain	26
5.2	Summary for mesh used in simulations	26
5.3	Fluid examples for Prandtl numbers considered in the present work	28
5.4	Summary of the turbulence models used in the present work	28
5.5	Selected test cases of the natural convection flow regime with RBC configuration.	29
A.1	Summary for parameters defining the three meshes used for analysis	47



# CONTENTS

<b>List of Figures</b>	<b>iii</b>
<b>List of Tables</b>	<b>v</b>
<b>1 Introduction</b>	<b>3</b>
1.1 Thermal Convection	3
1.1.1 Forced Convection	3
1.1.2 Natural Convection	4
1.1.3 Mixed Convection	4
1.2 Research Question	4
1.3 Objective of thesis.	5
1.4 Thesis Outline	5
<b>2 Numerical Methods</b>	<b>7</b>
2.1 Governing Equations	7
2.2 Finite Volume Method	7
2.2.1 Flux Integration	9
2.2.2 Source term	9
2.3 Time Discretization	10
2.4 Boussinesq Approximation	10
<b>3 Turbulence Modeling</b>	<b>13</b>
3.1 RANS Equations	13
3.2 Low Reynolds $k-\epsilon$ model	13
3.3 Reynolds Stress Model - Elliptic Blending	14
<b>4 Turbulent Heat Flux modeling</b>	<b>17</b>
4.1 Introduction	17
4.2 Defining Dimensionless numbers.	18
4.2.1 Rayleigh Number	18
4.2.2 Prandtl number	18
4.3 THF modeling	18
4.3.1 Simple Gradient Diffusion Hypothesis	18
4.3.2 SGDHD with constant $Pr_t$	19
4.3.3 SGDHD with varying $Pr_t$	20
4.3.4 Look-up Table	21
4.3.5 General Gradient Diffusion Hypothesis	21
4.3.6 WET Approach	21
4.3.7 Algebraic Turbulent Heat Flux Model	22
4.3.8 AHFM-NRG	23
4.3.9 Significance of model	23
4.4 Calibration	23

<b>5</b>	<b>Application Phase</b>	<b>25</b>
5.1	Computational Domain	25
5.2	Mesh details	26
5.3	Flow Parameters	27
5.4	Simulation Setting	28
5.5	Selection of test cases	28
5.5.1	Test Cases	28
5.5.2	DNS case setup	29
5.5.3	Case 1	30
5.5.4	Case 2	32
5.5.5	Case 3	35
5.5.6	Case 4	37
5.5.7	Case 5	39
5.5.8	Case 6	41
<b>6</b>	<b>Conclusion and Future scope of work</b>	<b>45</b>
6.1	Conclusion	45
6.2	Future Scope of work	46
<b>A</b>	<b>Appendix</b>	<b>47</b>
A.1	Mesh Sensitivity Analysis	47
A.2	Perturbations in Temperature for Pr 0.025	49
	<b>Bibliography</b>	<b>51</b>

# ACKNOWLEDGMENTS

First of all, I would like to thank Dr.Ir. Afaq Shams for giving me this wonderful opportunity to work on such interesting project and guiding and motivating me from throughout the my thesis. His constant motivation and very constructive criticism helped me make this work in its best form. Also I would like to thank Prof.Dr.Ir. Marc Gerritsma for his overall guidance in structuring my thesis and report and providing his very constructive and valuable feedback regarding my work. Next, I would like to thank Nuclear Research and Consultancy Group, Petten for letting me use their resources and conduct my project. Also I would like to thank Dr. Blaž Mikuž for giving me his valuable time during the start of my work at NRG. I would like to thank my colleagues Akshat, Danielle, Jeremy and Stephano and all other colleagues at NRG for their time for very constructive discussions. I would like to acknowledge all my thesis committee members for agreeing to give their valuable time for my assessment. I also acknowledge the support from the EDF team with the code and my doubts related to it. Also I would like to thank my friends Adwait, Abhidnya, Shreyash and Rohit for their moral support and constant motivation to me to finish my work as early as possible. Also I would like to thank all of my friends in Delft for constantly motivating and inspiring me to do well. Last but not the least, I would like to thank my parents and my sister Anuja for their constant motivation, love and for believing in me which helped sail through my Masters. Without their constant moral support, this work would not have been possible.

*Kunal Kanawade*  
*Delft, December 2019*



# 1

## INTRODUCTION

Globally, the demand for energy is increasing exponentially and at the same time we are facing a huge crisis in the form of global warming. The IPCC (International Panel on Climate Change) Fifth Assessment Report (AR5), Stocker et al., [7], reported that human influence has been the dominant cause for the global surface temperature rise in mid-20th century, warming the planet globally by  $0.85^{\circ}\text{C}$  from 1880 to 2012. Global temperature rise is already resulting into increase in sea level rise, floods, droughts, bio diversity loss and many other still unfolding risks to ecosystems across the planet. According to latest IPCC report, [8], to keep the global temperature increasing from  $1.5^{\circ}\text{C}$ , we have limited amount of carbon emission left. The report summarizes the global carbon emissions have to be reduced by 50% by 2032. It is required to find alternatives to fossil fuel to deal with greenhouse gas emissions. In such situation, to meet the global energy demand and reduce the Greenhouse gas emissions, Renewable and Nuclear energy sources are considered to be great options. Nuclear Energy Agency, [9] have suggested that nuclear plants for energy production can reduce 10% of total  $\text{CO}_2$  emissions. In nuclear applications, the safety of nuclear reactor, is of prime concern. From design and safety aspect, the cooling systems of the reactor are of utmost importance. The reactor is equipped with many safety system which include active as well as passive cooling systems. In case of passive cooling systems, the coolant in the reactor, carries away the heat developed in the reactor naturally. In nuclear industry, liquid metals are considered to be a great coolant option particularly for their high thermal conductivity. In most of the nuclear reactor designs in the Generation IV International Forum (GIF), the primary coolant is considered to be liquid metals, Generation International Forum, [10]. Hence understanding the heat transfer involved in the reactor for is important designing the nuclear reactor. The physical phenomenon involved in the cooling system is thermal convection.

### 1.1. THERMAL CONVECTION

Broadly thermal convection can be categorized into three categories: Forced, Natural and Mixed convection. In this section we will discuss these categories to understand the physics briefly involved in the thermal convection.

#### 1.1.1. FORCED CONVECTION

In forced convection, as the name suggests, the fluid is forced to move around in the system with the intention of increasing the heat transfer. The fluid motion in forced convection is generated externally with help of devices like pumps, suction devices or fan. Forced convection can be seen in most space heating devices,

central heating systems and cooling systems in industries.

### 1.1.2. NATURAL CONVECTION

In natural convection flows, the fluid is driven by buoyant forces. The buoyant forces in the fluid are generated due to the density difference which are created by the temperature gradient. In natural convection for flow circulation, temperature gradient, gravitational acceleration or presence of another acceleration, is required. In nuclear applications, natural convection is used extensively to remove the heat from the nuclear reactor. Also the natural convection based cooling systems are energy effective as no external source of energy is required to drive the fluid.

### 1.1.3. MIXED CONVECTION

In mixed convection flows, the heat transfer is done by both forced and mixed convection mechanisms. The pressure forces and buoyant forces both are responsible for the fluid motion. For mixed convection flows, the temperature gradient is necessary for the generation of buoyant forces and external source such as pump or suction device is required for providing the pressure forces. In nuclear reactors as well as heat exchangers, mixed convection application can be found.

## 1.2. RESEARCH QUESTION

In the nuclear applications, passive safety systems have been identified as one of the most cost effective safety systems. Passive safety systems in the nuclear reactor work on the principle of natural convection. The coolant is naturally heated by the source which leads to change in density of the fluid. Buoyant forces are generated due to the density change drive the fluid from one part of the reactor to another. Forced convection based cooling systems can break down completely in-case of emergency power shutdown whereas the passive safety systems based on natural convection, work in-spite of the power to the reactor and the mechanism that is removing the heat from the reactor works effectively in absence of external power source. Hence it is highly important to study the heat transfer by natural convection and be able to model heat transfer computationally. Natural convection is a process in which momentum and heat are transferred within the fluid flow due to the effects of buoyancy. This phenomenon represents an important mechanism of heat transfer involved in nuclear applications. With respect to natural convection, the buoyancy driven flow has been extensively studied numerically but the research was limited by the modeling capabilities of the existing models for thermal flow predictions.

Computational Fluid Dynamics (CFD) is a numerical approach that has been widely used for simulating fluid flows in aerospace, nuclear, marine and many other industries. CFD is a numerical approach to predict the flow phenomena. CFD studies employ different types of model to reproduce or predict the turbulence of the flow. CFD analysis is being used as reference data in making conceptual models in product development stage. Complex phenomenon which involve tremendous efforts to be done practically can be easily predicted by CFD analysis. In a standard CFD analysis, a physical model of the desired phenomenon is developed. The governing equations of the physical model are then solved using numerical techniques. Computationally expensive terms or equations are modeled by making suitable approximations. In the framework of present work, one of the such models for predicting accurate heat transfer is being dealt with.

For fluid flow modeling, the flow is governed by Navier-Stokes equations. For past several years, different approaches of solving these equations are being developed which include Direct Numerical Simulation (DNS), Large eddy simulations (LES), Reynolds Averaged Navier-Stokes (RANS) approach. These approaches mentioned account for different computational efforts. In industrial applications, RANS approach has been widely used due to its computational viability compared to other approaches. DNS being most computationally expensive is uncommon in industrial applications however it is powerful research tool in understanding

the turbulence at fundamental level [11]. Also DNS results are used as widely as reference data to validate, turbulence models developed in RANS or LES.

The Rayleigh Bénard convection (RBC) case is considered to be the prototypical case for the natural flow convection analysis. This physical case is defined by the Prandtl number and Rayleigh number of the flow. The buoyancy is generated by maintaining a constant temperature gradient across the differentially heated walls where the bottom wall is maintained at higher temperature than the lower wall. This case has been widely studied in various literature although with the studies limited by the inadequate modeling approaches used. Various DNS studies have undertaken these cases and have created bench-marking results for other modeling approaches to follow. DNS/LES being computationally expensive, can be very difficult and time consuming in employing for industrial applications.

In addition, it should be noted that the RANS approach of modeling turbulent momentum or heat fluxes in complex flows is still the most important approach as it accounts for less expensive and time optimal computations. In the same context, a large number of models have been proposed for the modeling the turbulent momentum fluxes such as eddy viscosity models and other RANS approaches. Turbulent heat flux modeling, on the contrary has not been able to attract the same attention from researchers. Most widely used turbulent heat fluxes (THF) closure, the Reynolds analogy is a robust and simplistic model. Although, this model is proven to be inadequate in thermal predictions of flow involving low-Prandtl fluids. The turbulent heat flux modeling plays an important role in thermal predictions of the flow, Desantis et al., [12]. Researchers subsequently moved on to develop more advanced models to overcome the drawbacks posed by the previous models, Shams et al., [13].

### 1.3. OBJECTIVE OF THESIS

The primary objective of the present work is to extend and calibrate the AHFM-NRG formulation for natural convection flow regimes coupled with Reynolds Stress Model Elliptic Blending (RSM-EB) for accurate turbulent heat flux prediction. Also present work aims to validate the model for different test cases of Rayleigh Bénard Convection, with reference data and investigate the effects of employing higher order turbulence model for thermal predictions.

### 1.4. THESIS OUTLINE

In Chapter 1, the importance of CFD analysis and its different numerical approaches are discussed briefly. It also discusses the thesis project objective. Governing equations of the physical phenomenon and computational experiment are discussed in Chapter 2. In this Chapter, dimensionless numbers defining the numerical experiment and other involved approximations are briefly explained. In Chapter 3, numerical methodology undertaken for the simulations will be discussed. In Chapter 4, the AHFM-NRG+ model has been extended for natural convection flows by calibrating the model coefficients. Also this chapter describes the computational experiment elements such mesh type, boundary conditions, numerical schemes, turbulence and turbulent heat flux models. In Chapter 5, different test cases in the thesis project and results obtained from the simulations are discussed. In Chapter 6, aims to briefly explain future scope of work, summarize the observations, conclude from the present work.



# 2

## NUMERICAL METHODS

The fluid flow movement is determined by a set of governing equations. Depending upon the physical conditions, phases of fluid involved and assumptions made for simplifying the flow study, different equations are considered. In this chapter, the equations involved in the current work are discussed. Also different numerical schemes, used in discretization of space and time variable in solving these equations and time stepping methods are discussed too.

### 2.1. GOVERNING EQUATIONS

In this section, the equation governing the fluid flow movement are discussed briefly. The physical law of conservation of mass, energy and momentum are translated in their mathematical form in terms of partial differential equations, and are known as Navier-Stokes equations [14, 15]. With the help of these equations, wide range of flow configurations are modeled numerically. Broadly the fluid flows based in the level of turbulence involved, are categorized as laminar and turbulent flows. These flows are defined by the physical quantities like velocity, pressure and temperature. In this section, within the framework of current project, incompressible flow equations are dealt and hence following equations are valid for incompressible fluid flows. The conservation of mass is mathematically expressed as given in Equation (2.1) and is also known as Continuity equation. The conservation of momentum is mathematically expressed in Equation (2.2) and conservation of energy in Equation (2.3).

$$\frac{\partial \rho}{\partial t} + \frac{\partial \rho u_i}{\partial x_i} = 0, \quad (2.1)$$

$$\frac{\partial \rho u_j}{\partial t} + \frac{\partial \rho u_i u_j}{\partial x_i} = \frac{\partial T_{ij}}{\partial x_i} + \rho f_j, \quad (2.2)$$

$$\frac{\partial \rho E}{\partial t} + \frac{\partial \rho E u_i}{\partial x_i} = \frac{\partial T_{ij} u_j}{\partial x_i} - \frac{\partial q_i}{\partial x_i} + \rho f_i u_j, \quad (2.3)$$

where  $T_{ij}$  denotes the stress tensor of Newtonian fluid and  $q_i = k \frac{\partial T}{\partial x_i}$  heat flux by Fourier's law. For accurately describing a fluid flow, various numerical techniques are employed. In coming sections, these approaches and numerical techniques are discussed briefly.

### 2.2. FINITE VOLUME METHOD

In the framework of present work, *Code\_Saturne* has been employed for numerical simulations as CFD solver and the solver in the code is based on finite volume method of discretization. Hence, in this section,

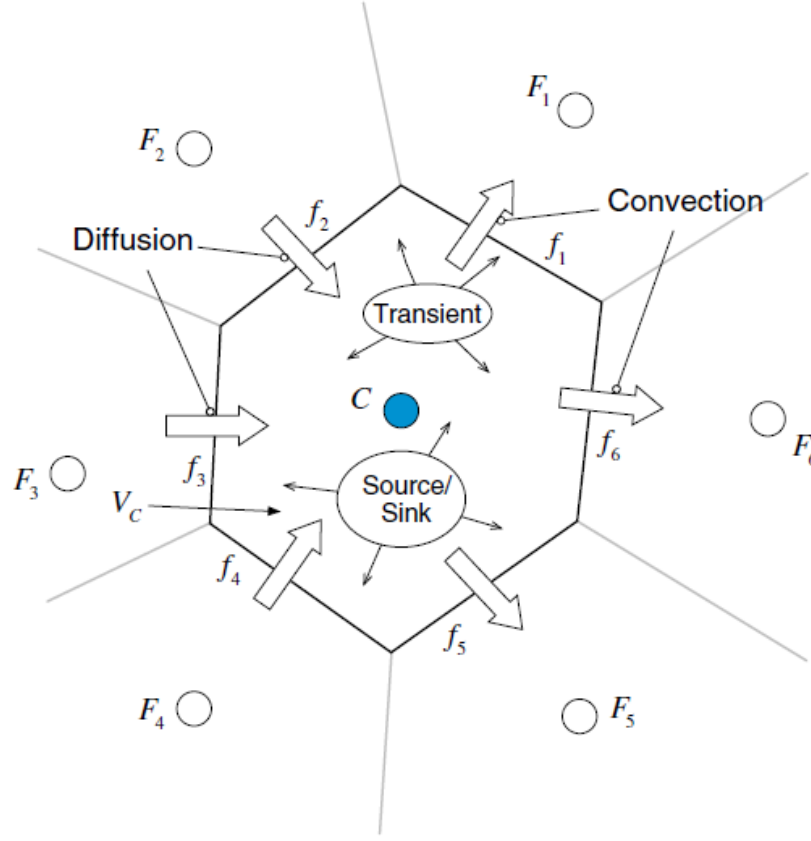


Figure 2.1: Conservation in a discrete element

the finite volume method is discussed briefly in order to get idea of the numerics involved in the numerical simulations. Numerical methods are developed for calculations for flow simulations for a given domain. The domain is discretized using finite volume method for describing the Navier-Stokes partial differential equations into a system of linear algebraic equations. The physical domain of the flow is discretized into smaller volume elements. The given partial differential equations are integrated over an element by transforming the surface and volume integral into algebraic equations. Interpolation schemes are used to interpolate the variation of equation variables within the volume element and relate the surface values to the cell volume values. The finite volume method is widely used in CFD calculations as the physical domain of the given problem is same as the computational domain for numerical simulations.

The finite volume method (FVM) is based on conservation principle hence the conservative form of equation is considered here. Let's consider an element  $C$  with general scalar quantity  $\phi$  and the transport equation in conservative form integrating over the element  $C$  can be written as follows:

$$\int_{V_c} \nabla \cdot (\rho \mathbf{v} \phi) dV = \int_{V_c} \nabla \cdot (\Gamma^\phi \nabla \phi) dV + \int_{V_c} Q^\phi dV. \quad (2.4)$$

By Gauss's theorem, the volume integrals can be replaced by surface integrals as follows:

$$\oint_{\partial V_c} (\rho \mathbf{v} \phi) \cdot \vec{dS} = \oint_{\partial V_c} (\Gamma^\phi \nabla \phi) \cdot \vec{dS} + \int_{V_c} Q^\phi, dV \quad (2.5)$$

where the term on the left denotes the convective term and in left hand side, the first term denotes the diffusion term whereas the term with  $Q^\phi$  denotes the source term for the scalar quantity  $\phi$ ,  $\mathbf{v}$  is velocity and  $V_c$  volume of the cell. The surface integral of the fluxes is calculated on the surface of the control volume  $C$ . The convective and diffusive fluxes are summation of all the surface integrals of diffusive and convective fluxes at each face of the control volume  $C$ .

### 2.2.1. FLUX INTEGRATION

In this section, the flux integration of over the faces of the control volume is discussed. The surface integrals over cell volume C are summation of all the integrals at all the surfaces of volume C. Lets denote convective and diffusion fluxes as follows:

$$J^{\phi,C} = \rho v \phi, \quad (2.6)$$

$$J^{\phi,D} = -\Gamma^{\phi} \nabla \phi, \quad (2.7)$$

Total flux can be defined as

$$\oint_{\partial V_c} J^{\phi,C} \cdot \vec{dS} = \sum_{f_1}^{f_n} \left( \int_f (\rho \vec{v} \phi) \cdot \vec{dS} \right), \quad (2.8)$$

$$\oint_{\partial V_c} J^{\phi,D} \cdot \vec{dS} = \sum_{f_1}^{f_n} \left( \int_f (\Gamma^{\phi} \nabla \phi) \cdot \vec{dS} \right). \quad (2.9)$$

Applying Gaussian quadrature rule at the integral of the face f of the cell volume , we have :

$$\int_f J^{\phi} \cdot \vec{dS} = \int_f (J^{\phi} \cdot \vec{n}) dS = \sum_{ip(f)} (J^{\phi} \cdot \vec{n})_{ip} \omega_{ip} S_f \quad (2.10)$$

where  $ip$  denotes the integration point and  $ip(f)$  denotes the number of integration along surface f. Number of integration points are determined by the required accuracy of the solution. In case of one integration point situated at center of C and weighing function  $\omega_{ip}$  is taken as 1 then the mean value integration rule is derived. It is also known as trapezoidal rule which is second order accurate. With two integration points for  $\omega_{ip}$  as 1/2 would be third order accurate. With increase in integration points, the accuracy order increases. Finally the flux integrals can be written as follows:

$$\oint_{\partial V_c} (\rho \vec{v} \phi) \cdot \vec{dS} = \sum_{f \in \text{aces}(V)} \sum_{ip(f)} \left( \omega_{ip} (\rho v \phi)_{ip} \cdot S_f \right) \quad (2.11)$$

$$\oint_{\partial V_c} (-\Gamma \nabla \phi) \cdot \vec{dS} = \sum_{f \in \text{aces}(V)} \sum_{ip(f)} \left( \omega_{ip} (-\Gamma \nabla \phi) \cdot S_f \right) \quad (2.12)$$

### 2.2.2. SOURCE TERM

In this section, the volume integral for the source term is discussed. Applying Gaussian quadrature integration, the volume integral of the source term can be written as:

$$\int_V Q^{\phi} dV = \sum_{ip} \left( Q_{ip}^{\phi} \omega_{ip} V \right) \quad (2.13)$$

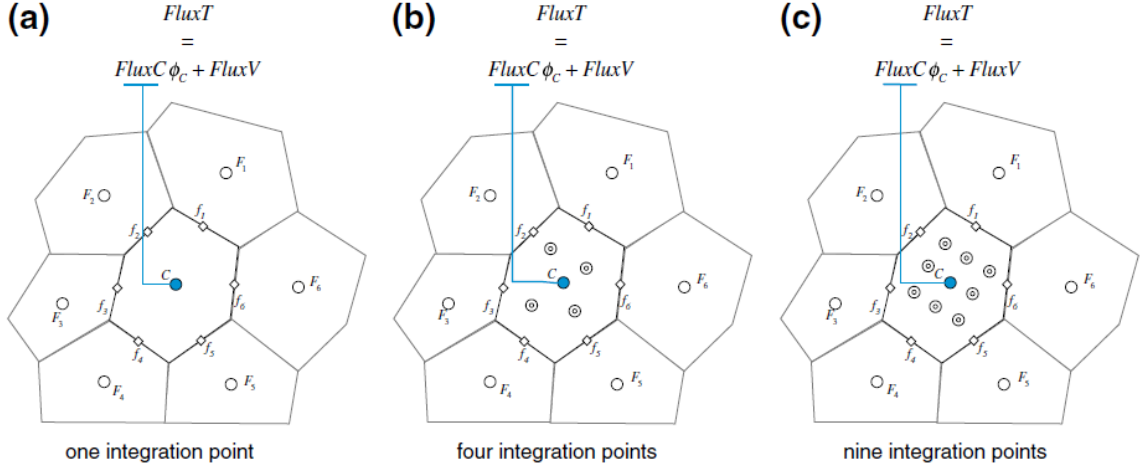


Figure 2.2: Varying integration points for source integrals

In this case also the accuracy of the solution depends on the number of integration points are used. In case of one integration point situated at the center of element and  $\omega_{ip}$  as 1 the approximation would be second order accurate. This approximation is widely popular in two and three dimensional cases. As the number of integration points increase, the accuracy increases with  $\omega_{ip}$  function properly distributed among the integration points.

### 2.3. TIME DISCRETIZATION

In steady state solutions, the system of equations do not have transient term. In case of steady state flows, the flow calculations are done for the mean solution independent of time consideration. In presence of a transient term in the equations, it needs to be discretized with appropriate time stepping method. In a typical solution to transient system, the solution is initialised at  $t = t_0$  and solver moves ahead to find solution at  $t_1 = t_0 + \Delta t_1$ . Subsequently it moves ahead with the initial condition as solution found at  $t_1$  and solution is found at  $t_2 = t_1 + \Delta t_2$ . The similar iterative procedure is followed to reach the desired time. Broadly the the temporal discretization can be categorized in Implicit and explicit method.

### 2.4. BOUSSINESQ APPROXIMATION

In thermal convection cases like Rayleigh Bénard Convection flow regimes, the flow is driven by the buoyant forces created in the flow due to the temperature gradient across two walls in the domain. In such flow cases, the incompressible fluid is to be simulated as a compressible fluid in the simulation. The fluid experiences buoyant forces although the forces due to inertia are not considered. J Boussinesq proposed set of approximations to simplify the equations governing the motion of buoyant forces, Boussinesq, [16]. In his work, he proposed following key approximations:

- Fluid properties are considered constant.
- Fluid flow of interest had been considered to be incompressible
- The energy equation is considered to be decoupled from flow mechanical energy.

Incompressible flows refer to the negligible or no density change during the flow movement of the fluid. in case of arge temperature differences, where the change in density is not negligible like Flows with Mach number higher than 0.3 , unsteady flow with varying pressure and density with respect to time and space

and pressure variations caused due to height. Boussinesq approximation lets us account for the change in density without solving compressible Navier-Stokes equations. In case of incompressible fluid flows, the density is not solved for, similarly with boussinesq approximation, the density is considered to be a function of temperature but is not solved for in the simulation calculations. This approximation has been widely used in number of numerical simulations. The implementation of this approximation has helped reduce computational costs for solving full compressible Navier-Stokes equations. The mathematical implementation of Boussinesq equation, the properties of the fluid are considered constant and the density variation is calculated with the difference of change in temperature from reference temperature. The mathematical form of the Boussinesq approximation can be written as follows:

$$\rho = \rho_0[1 - \beta(T - T_0)] \quad (2.14)$$

where  $\rho_0$  is density of the fluid at reference temperature  $T_0$ ,  $\beta$  is thermal expansion coefficient of fluid and  $T$  is the temperature of the fluid. Now lets consider unsteady Navier-Stokes equation:

$$\nabla \cdot \vec{u} = 0 \quad (2.15)$$

$$\frac{Du}{Dt} = -\frac{1}{\rho_0} \frac{\partial p}{\partial x} + \nu \nabla^2 u \quad (2.16)$$

$$\rho_0 \frac{Dv}{Dt} = \frac{\partial p}{\partial y} - \rho g + \mu \nabla^2 v \quad (2.17)$$

$$\frac{Dw}{Dt} = -\frac{1}{\rho_0} \frac{\partial p}{\partial z} + \nu \nabla^2 w \quad (2.18)$$

$$\frac{DT}{Dt} = \alpha \nabla^2 T \quad (2.19)$$

where  $\alpha$  is thermal diffusivity,  $g$  is gravity acting in downward y-direction. Now the implementation of the Boussinesq approximation is done for  $\rho$  in y-direction momentum equation to account for the buoyant forces generated due to gravity  $g$ . And we have:

$$\rho_0 \frac{Dv}{Dt} = \frac{\partial p}{\partial y} - \rho_0[1 - \beta(T - T_0)]g + \mu \nabla^2 v \quad (2.20)$$

Now to simplify this equation further we approximate the  $\frac{\partial p}{\partial y}$  in boundary layer such that the pressure gradient across y direction is defined by hydro-static pressure gradient as the flow in natural convection regime does not have any external forces hence this approximation can be considered to be valid:

$$\frac{\partial p}{\partial y} = -\rho_0 g \quad (2.21)$$

From equations 2.20 and 2.21, we have

$$\rho_0 \frac{Dv}{Dt} = \rho_0 g - \rho_0 g - \rho_0 \beta(T - T_0)g + \mu \nabla^2 v \quad (2.22)$$

$$\rho_0 \frac{Dv}{Dt} = \rho_0 \beta(T - T_0)g + \mu \nabla^2 v \quad (2.23)$$

$$\rho_0 \frac{Dv}{Dt} = \beta(T - T_0)g + \nu \nabla^2 v \quad (2.24)$$



# 3

## TURBULENCE MODELING

In this section, the Reynolds-averaged Navier-Stokes equations are discussed. These equations are then employed in CFD solver to perform simulations in the framework of the present thesis project.

### 3.1. RANS EQUATIONS

Reynolds averaged Navier-Stokes equations solve for the mean velocity of the flow of incompressible fluids. Reynolds proposed that the velocity of any fluid can be decomposed into mean velocity and its fluctuation. In most of the numerical simulations, RANS approach is employed for its robustness and accuracy at low computational efforts as compared to DNS or LES approaches. Following equations describe the Reynolds averaged Navier-Stokes continuity and momentum equations for incompressible flows:

$$\frac{\partial U_i}{\partial x_i} = 0 \quad (3.1)$$

$$\rho \frac{\partial U_i}{\partial t} + \rho U_j \frac{\partial U_i}{\partial x_j} = -\frac{\partial P}{\partial x_i} + \frac{\partial}{\partial x_j} (2\mu S_{ij} - \rho \overline{u'_i u'_j}) \quad (3.2)$$

where  $U_i$  denotes the average velocity and  $\overline{u'_i u'_j}$  is Reynolds Stress term ( $\tau_{ij}$ ) which is also known as turbulent momentum flux (TMF). It is required to model this TMF terms in order to close the system of ten flow variables with four equations. In 1903, Boussinesq, [16], proposed to model this tensor with the eddy viscosity. He suggested that the Reynolds Stress term is related to the mean strain rate with eddy viscosity.

$$\tau_{ij} = 2\mu_t S_{ij} - \frac{2}{3}\delta_{ij}k \quad (3.3)$$

where  $k$  is turbulent kinetic energy,  $\delta_{ij}$  is Kronecker delta and  $S_{ij}$  is mean shear strain rate which is expressed by following expression:

$$S_{ij} = \frac{1}{2} \left( \frac{\partial U_i}{\partial x_j} + \frac{\partial U_j}{\partial x_i} \right) - \frac{1}{3}\delta_{ij} \frac{\partial U_k}{\partial x_k} \quad (3.4)$$

### 3.2. LOW REYNOLDS K- $\epsilon$ MODEL

In this section the low Reynolds  $k-\epsilon$  model is discussed which has been as used in the framework for the thesis project. The low-Re  $k-\epsilon$  model is given by Lien et al., [17]. Launder et al., [18] proposed the first formulation of  $k-\epsilon$  model which is based on the principle of equilibrium between turbulent production and dissipation. This model presents a very good agreement for the external flows but has limitations with higher pressure

gradients. The eddy viscosity model which are formulated on the basis of linear Boussinesq relation have the tendency to not capture the non-isotropic nature of the flow and high turbulence generation in case for impinging conditions. To overcome the drawbacks posed by former k- $\epsilon$  formulations, an approach based on relating Reynolds stress term and strains are required for low-Re regions in the flow. The following equations explain the transport equations for k and  $\epsilon$  :

$$\frac{D(\rho k)}{Dt} = P_k + P_b - \rho \epsilon + \frac{\partial}{\partial x_j} \left[ \left( \mu + \frac{\mu_t}{\sigma_k} \right) \frac{\partial k}{\partial x_j} \right], \quad (3.5)$$

$$\frac{D(\rho \epsilon)}{Dt} = \frac{C_{\epsilon_1}}{\tau} (P_k + P_{wall} + C_{\epsilon_3} P_b) - \rho C_{\epsilon_2} F_2 \frac{\epsilon}{\tau} + \frac{1}{\tau} \rho S_y + \frac{\partial}{\partial x_j} \left[ \left( \mu + \frac{\mu_t}{\sigma_\epsilon} \right) \frac{\partial \epsilon}{\partial x_j} \right], \quad (3.6)$$

where

$$P_{wall} = DF_2 \left( P_k + 2\mu \frac{k}{d^2} \right) \exp(-ERe_d^2), \quad (3.7)$$

$$f_\mu = 1 - \exp \left[ - \left( C_{d_0} \sqrt{Re_d} + C_{d_1} Re_d + C_{d_2} Re_d^2 \right) \right], \quad (3.8)$$

$$F_2 = [1 - C \exp(Re_t^2)], \quad (3.9)$$

$$S_y = C_w \frac{\epsilon^2}{k} \max \left[ \left( \frac{\ell}{\ell_\epsilon} - 1 \right) \left( \frac{\ell}{\ell_\epsilon} \right)^2, 1 \right], \quad (3.10)$$

$$\ell = \frac{k^{3/2}}{\epsilon}, \quad (3.11)$$

$$\ell_\epsilon = C_\ell d, \quad (3.12)$$

and the turbulent viscosity  $\mu_t$  is evaluated as

$$\mu_t = \nu_t \rho = \rho f_\mu C_\mu k \tau, \quad (3.13)$$

In the equations above  $P_k = -\rho \overline{u_i u_j} \partial U_i / \partial x_j$  and  $P_b = -\rho \beta g_i \overline{u_i t}$  represent the turbulence production due to the mean strain and buoyancy, respectively,  $\tau = \max \left( \frac{k}{\epsilon}, C_t \sqrt{\frac{\nu}{\epsilon}} \right)$  is the turbulent mechanical time scale,  $d$  is the wall distance,  $Re_d = \sqrt{k} d / \nu$  and  $Re_t = k^2 / \nu \epsilon$ . In addition, the so-called Yap correction, to reduce the departure of the turbulence length scale from its local equilibrium level, is included in the transport equation of the turbulent dissipation rate through the source term  $S_y$ , Yap et al., [19].

### 3.3. REYNOLDS STRESS MODEL - ELLIPTIC BLENDING

Reynolds Stress Model- Elliptic Blending (RSM-EB) turbulence model was originally given by Manceau et al., [20], in 2002. In this section, the formulation of RSM-EB that is adopted in *Code\_Saturne* is discussed. The transport model for Reynolds stress is as follows:

$$\frac{D(\rho \overline{u_i u_j})}{Dt} = P_{ij} + P_{b,ij} + D_{t,ij} + \phi_{ij} - \epsilon_{ij} + \frac{\partial}{\partial x_k} \left( \mu \frac{\partial \overline{u_i u_j}}{\partial x_k} \right), \quad (3.14)$$

where  $P_{ij}$  denotes mechanical production,  $P_{b,ij}$  denotes production caused by buoyancy,  $D_{t,ij}$  denotes turbulent diffusion,  $\phi_{ij}$  denotes pressure-strain correlation and  $\epsilon_{ij}$  denotes dissipation.

The mechanical production term is given by:

$$P_{ij} = -\rho (\overline{u_i u_k} \frac{\partial U_j}{\partial x_k} + \overline{u_j u_k} \frac{\partial U_i}{\partial x_k}), \quad (3.15)$$

whereas production due to buoyancy is given by:

$$P_{b,ij} = -\rho\beta(g_i\overline{\theta u_j} + g_j\overline{\theta u_i}) \quad (3.16)$$

The turbulent diffusion term is given by the Simple Gradient Diffusion Hypothesis (SGDH) as follows:

$$D_{t,ij} = \frac{\partial}{\partial x_k} \left( \frac{\mu_t}{\sigma_k} \frac{\partial \overline{u_i u_j}}{\partial x_k} \right), \quad (3.17)$$

and turbulent viscosity  $\mu_t$  is given by:

$$\mu_t = \rho C_\mu \frac{k^2}{\varepsilon}. \quad (3.18)$$

The pressure strain and the dissipation term are modeled in a blending of near wall and high Reynolds model, due to which the model is called as Elliptic Blending, are given by:

$$\phi_{ij} - \varepsilon_{ij} = (1 - \alpha^3) (\phi_{ij}^w - \varepsilon_{ij}^w) + \alpha^3 (\phi_{ij}^h - \varepsilon_{ij}^h), \quad (3.19)$$

where the superscript  $^h$  and  $^w$  denote high Reynolds and near-wall formulations respectively. The blending parameter  $\alpha$  is solved for from the following equation:

$$\alpha - \ell^2 \nabla^2 \alpha = 1. \quad (3.20)$$

The pressure-strain and dissipation terms for the near-wall formulation, are:

$$\phi_{ij}^w = -5\rho \frac{\varepsilon}{k} \left( \overline{u_i u_k} n_j n_k + \overline{u_j u_k} n_i n_k - \frac{1}{2} \overline{u_k u_l} n_k n_l (n_i n_j + \delta_{ij}) \right), \quad (3.21)$$

$$\varepsilon_{ij} = \rho \overline{u_i u_j} \frac{\varepsilon}{k}. \quad (3.22)$$

The gradient of the blending parameter is used to calculate the wall normal vector :

$$n_k = \frac{\frac{\partial \alpha}{\partial x_k}}{\sqrt{\frac{\partial \alpha}{\partial x_l} \frac{\partial \alpha}{\partial x_l}}}. \quad (3.23)$$

Now for the higher-Reynolds formulation, Reynolds, [6]:

$$\phi_{ij}^h = -\left( C_1 + C_1^* \frac{1}{2} \frac{P_{ii}}{\varepsilon} \right) \varepsilon a_{ij} + (C_3 + C_3^* \sqrt{a_{kl} a_{kl}}) k S_{ij} + C_4 k \left( a_{ik} S_{jk} + a_{jk} S_{ik} - \frac{2}{3} a_{lm} S_{lm} \delta_{ij} \right) + C_5 k (a_{ik} W_{jk} + a_{jk} W_{ik}), \quad (3.24)$$

where

$$a_{ij} = \frac{\overline{u_i u_j}}{k} - \frac{2}{3} \delta_{ij}, \quad (3.25)$$

$$S_{ij} = \frac{1}{2} \left( \frac{\partial U_i}{\partial x_j} + \frac{\partial U_j}{\partial x_i} \right), \quad (3.26)$$

$$W_{ij} = \frac{1}{2} \left( \frac{\partial U_i}{\partial x_j} - \frac{\partial U_j}{\partial x_i} \right), \quad (3.27)$$

and

$$\varepsilon_{ij}^h = \frac{2}{3} \rho \varepsilon \delta_{ij}. \quad (3.28)$$

Now the transport equation for the turbulent kinetic energy dissipation rate  $\varepsilon$  is as follows:

$$\frac{D\rho\varepsilon}{Dt} = \frac{1}{\tau} \left( \frac{C_{\varepsilon 1}}{2} (P_{ii} - C_{\varepsilon 3} P_{b,ii}) - C_{\varepsilon 2} \rho \varepsilon \right) + \frac{\partial}{\partial x_k} \left( \left( \mu + \frac{\mu_t}{\sigma_\varepsilon} \right) \frac{\partial \varepsilon}{\partial x_k} \right) + \rho S_E, \quad (3.29)$$

where  $S_E$  is added to recreate the near-wall behavior of dissipation rate and is as follows:

$$S_E = A_1 \nu \overline{u_k u_l} n_k n_l \frac{k}{\varepsilon} (1 - \alpha^3) \left( \frac{\partial S_{ij} n_i n_k}{\partial x_k} \right)^2. \quad (3.30)$$

Table 3.1 describes the values of the model coefficients used in the above formulation:

$C_{\varepsilon 1}$	1.44	$A_1$	0.085	$C_3$	0.8
$C_{\varepsilon 2}$	1.83	$C_t$	6	$C_3^*$	0.65
$C_{\varepsilon 3}$	-0.33	$C_l$	0.133	$C_4$	0.625
$C_\mu$	0.07	$C_\eta$	80	$C_5$	0.2
$\sigma_k$	1.0	$C_1$	1.7		
$\sigma_\varepsilon$	1.5	$C_1^*$	0.9		

Table 3.1: Model coefficients for RSM-EB formulation [6]

# 4

## TURBULENT HEAT FLUX MODELING

In the RANS approach, the energy equation has a non-linear unknown heat flux term. In order for an appropriate closure of the system, models are introduced for closing the non-linear terms. In this chapter the different approaches of the turbulent heat flux modeling will be discussed.

### 4.1. INTRODUCTION

In a numerical experiment, it is highly impervious to model turbulent momentum fluxes and turbulent heat fluxes as correctly as possible to get a reliable thermal and flow field prediction. Due to its wide applications in industry, a RANS approach has always been researched upon a lot by researchers. Many RANS turbulence models have been developed to predict the turbulence involved in flow simulations. For governing the in-comprehensible turbulent flows Reynolds-averaged momentum and energy equations are as follows:

$$\frac{DU_i}{Dt} = F_i - \frac{1}{\rho} \frac{\partial P}{\partial x_i} + \frac{\partial}{\partial x_j} \left( \nu \frac{\partial U_i}{\partial x_j} - \overline{u_i u_j} \right), \quad (4.1)$$

$$\frac{DT}{Dt} = \frac{q}{\rho c_p} + \frac{\partial}{\partial x_j} \left( \frac{\nu}{\sigma_T} \frac{\partial T}{\partial x_j} - \overline{\theta u_i} \right), \quad (4.2)$$

where  $\frac{D}{Dt} = \frac{\partial}{\partial t} + U_k \frac{\partial}{\partial x_k}$  is the material derivative,  $F_i$  is the body force and  $q$  is the internal energy source. Although the turbulent heat flux modeling has not been given the equal amount of emphasis in terms of research. Consequently, the most simplistic yet robust, Simple Gradient Diffusion Hypothesis (SGDH) model is employed in most of the thermal numerical calculations as THF model. The model calculates the unknown turbulent thermal diffusivity by making use of Reynolds Analogy approach where thermal diffusivity is calculated as the ratio of turbulent viscosity  $\mu_t$  and turbulent Prandtl number  $Pr_t$ . Owing to the known limitations of this model, such as inability to capture buoyant forces and its application for low Prandtl fluids new models were developed. Statistically, the momentum and thermal boundary layer exhibit similar trends in terms of fluctuations and thickness for fluids with Prandtl number close to one. Fluids with low Prandtl number are characterized by relatively higher thermal diffusivity as compared to the momentum diffusivity leading to dissimilar momentum and thermal boundary layer thickness. In such cases the Reynolds Analogy approach i.e. SGDH fails to predict the accurate thermal field. To overcome the limitations posed by such a simplistic approach, sophisticated turbulent heat flux modeling approaches have to be employed. In the next sections, dimensionless numbers defining the case and turbulent heat flux modeling are discussed to understand the models employed in the framework of current thesis project.

## 4.2. DEFINING DIMENSIONLESS NUMBERS

The Rayleigh Bénard Convection case is defined by Rayleigh and Prandtl numbers. Before we dive into the turbulent heat flux modeling, the non-dimensional numbers and their physical significance in defining the case will be discussed.

### 4.2.1. RAYLEIGH NUMBER

Rayleigh number (Ra), for a flow is associated with buoyancy-driven flow such as natural convection flow regimes. Rayleigh number is represented by the ratio of buoyant forces in the fluid and to the viscous force. In the framework of current project, Rayleigh Bénard Convection case of natural convection is considered here. Due to the temperature gradient, the heated fluid at the bottom resulting in lower density, tends to move upward and fluid with relatively higher velocity tends to move down in the presence of gravity acting downwards. At relatively low value of Rayleigh number, the viscous forces are more dominant than buoyant forces, there isn't any movement in the fluid. The heat transfer occurs only through conduction. Above a certain value of Ra, which is called as critical Rayleigh number, the fluid movement and heat transfer occurs by natural convection [21]. Rayleigh number is defined as follows:

$$Ra = \frac{g\beta\Delta TH^3}{\nu\alpha}, \quad (4.3)$$

where  $g$  is gravitational acceleration,  $\beta$  is thermal expansion coefficient,  $H$  is characteristic length,  $\nu$  is kinematic viscosity and  $\alpha$  is thermal diffusivity which is defined as

$$\alpha = \frac{k}{\rho c_p}, \quad (4.4)$$

where  $k$  is thermal conductivity,  $\rho$  is density and  $c_p$  is specific heat of fluid at constant pressure.

### 4.2.2. PRANDTL NUMBER

Prandtl number (Pr) of a fluid is defined as ratio of its momentum diffusivity and thermal diffusivity. The Pr is defined as follows:

$$Pr = \frac{c_p\mu}{k}, \quad (4.5)$$

where  $c_p$  is specific heat of fluid at constant temperature,  $\mu$  is dynamic viscosity and  $k$  is thermal conductivity. Fluids with small Pr values i.e.  $Pr \ll 1$ , are generally called as low-Pr fluids. For low-Pr fluids, the thermal diffusivity is relatively higher than momentum diffusivity. For such fluids, the heat transferred by conduction is way more than convection. Hence they make excellent choice as coolants in nuclear applications. Low-Pr fluid examples include molten metals such as mercury, molten potassium and molten lithium. Fluids with high Pr values i.e.  $Pr \gg 1$ , have heat diffusion occur at slower rate than momentum diffusion. High-Pr fluid examples include engine oil, glycerol and refrigerant.

## 4.3. THF MODELING

In this section different approaches for THF modeling will be discussed briefly. The evolution of the turbulent heat flux models and their different formulations will be discussed which will help in understanding the AHFM-NRG+ model.

### 4.3.1. SIMPLE GRADIENT DIFFUSION HYPOTHESIS

In this section, the Reynolds Analogy approach i.e. Simple Gradient Diffusion Hypothesis (SGDH) model has been discussed in detail. Following expression summarizes SGDH approach mathematically:

$$\overline{\theta u_i} = -\frac{\nu_t}{Pr_t} \frac{\partial T}{\partial x_i}, \quad (4.6)$$

where  $\nu_t$  is the eddy viscosity and for a two-equation  $k - \epsilon$  model can be defined as  $C_\mu k^2/\epsilon$ :  $k$  is turbulent kinetic energy and its  $\epsilon$  is dissipation rate. From the above expression it can be observed that the model assumes that the turbulent Prandtl number  $Pr_t$  being constant throughout the domain. However,  $Pr_t$  is not constant for fluids and liquid metals, A.Shams, [22]. Hence this model does not accurately represent the turbulent heat fluxes. For low Prandtl fluids this model fails to agree with reference data for thermal field prediction, Roelofs et al., [5]. Few approaches with varying  $Pr_t$  [3, 4] were also proposed by many researchers. Although the thermal predictions showed some improvements against the conventional Reynolds analogy approach, it still showed deviations from reference data.

#### 4.3.2. SGDH WITH CONSTANT $Pr_t$

Widely in the CFD solvers the value of  $Pr_t$  is taken as 0.85 or 0.9. This approach works well for the  $Pr = 1$  but for the flows with  $Pr$  less than 1 i.e. in the case of liquid metals it does not predict the temperature field that well. Figure 4.1 describes that this approach works well for fluids with  $Pr = 1$  whereas shows deviation for Prandtl number less than 1 i.e.  $Pr = 0.025$  with respect to reference DNS data.

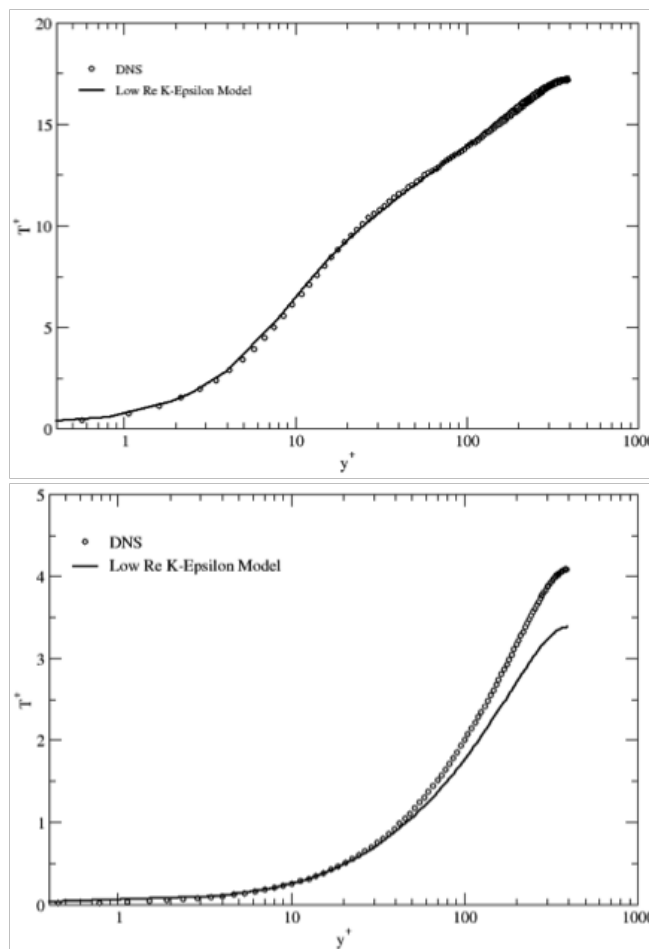


Figure 4.1: Evolution of mean temperature profile for  $Re_\tau = 395$  at (Left)  $Pr=1$  and (Right)  $Pr=0.025$ .

### 4.3.3. SGDH WITH VARYING $Pr_t$

Reynolds, [1], proposed varying  $Pr_t$  to SGDH model approach to overcome the above mentioned drawback and gave following relationship:

$$Pr_t = \left(1 + 100Pe^{-\frac{1}{2}}\right) \left(\frac{1}{1 + 120Re^{-\frac{1}{2}}} - 0.15\right), \quad (4.7)$$

where  $Re$  is bulk Reynolds number and  $Pe$  is Péclet number of the flow, which is defined as  $Pe = Re Pr$ , where  $Pr$  is Prandtl number and  $Re$  is Reynolds number of the flow.

Kays, [2], defined turbulent local  $Pr_t$  with another approach. It is calculated by turbulent Péclet number, defined as  $Pe_t = \frac{v_t}{\alpha}$  where  $\alpha$  is the thermal diffusivity, which is as follows :

$$Pr_t = 0.85 + \frac{0.7}{Pe_t}. \quad (4.8)$$

Further development to this, Weigand et al., [3], suggested dependence of the local  $Pr_t$  on the value of  $Pr_{t\infty}$  denotes the value of  $Pr_t$  for region far away from the wall in the fluid domain. It was defined as follows:

$$Pr_{t\infty} = 0.85 + \frac{100}{Pr Re^{0.888}}. \quad (4.9)$$

And the correlation is as follows:

$$\frac{1}{Pr_t} = \frac{1}{2Pr_{t\infty}} + CPe_t \frac{1}{\sqrt{Pr_{t\infty}}} - (CPr_{t\infty})^2 \left[1 - \exp\left(-\frac{1}{CPr_{t\infty}\sqrt{Pr_{t\infty}}}\right)\right], \quad (4.10)$$

where  $C=0.3$ . From equation (4.10), it can be seen that this correlation mixes the local and global parameters such as. It can be highlighted that in this correlation the local quantities have dependency on the global values as  $Pr_{t\infty}$  and, is a function of bulk Reynolds number.

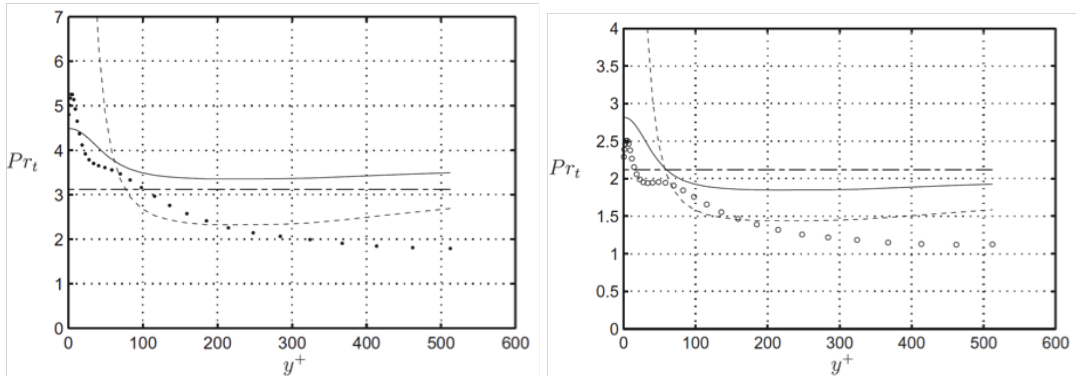


Figure 4.2: Models for  $Pr_t$  number compared to the LES for  $Re_\tau = 590$  at (Left)  $Pr=0.01$  (.) and (Right)  $Pr=0.025$ (o): Reynolds [1](dash-dot), Kays [2](dash) and Weigand et al. [3](solid) [4].

For liquid metals, the near wall region was studied by Duponcheel et al. [4] to derive a wall function for thermal field. Inspiration for this relation is taken from Kays and is as follows:

$$T^+ = \frac{Pr_t}{k} \log\left(1 + \frac{k}{Pr_t} Pr y^+\right). \quad (4.11)$$

For the above, it follows that the turbulent and molecular diffusivity are neglected and turbulent diffusivity is considered to be linear. Hence, it is called as mixed law-of-the-wall.

As we all know that the liquid metals do not exhibit constant  $Pr_t$  behavior throughout the domain. Kays [2] devised a correlation (4.8) for calculating the local  $Pr_t$  values in the domain as a function of turbulent Péclet number. Equation (4.8) is able to predict the values of  $Pr_t$  in better manner for the bulk region of the

fluid. Roelofs et al. [5] used Kays correlation for a channel flow case. In this case, the fluid has  $Pr=0.01$  and the results obtained are better than basic temperature gradient approach (SGDH). Although these results when compared with reference LES, fails to agree as seen from the Figure 4.3.

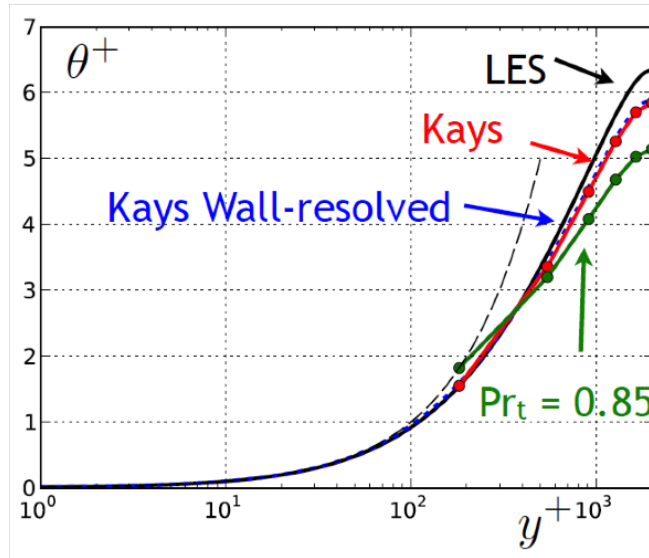


Figure 4.3: Temperature profiles of RANS at  $Re = 2000$  LES (black solid), linear law and  $Pr_t = 0.85$  (green), linear law  $\theta^+ = Pr_t \cdot y^+$  (black dashed), wall-resolved RANS with Kays correlation (blue), mixed law-of-the-wall and Kays (red). [5].

#### 4.3.4. LOOK-UP TABLE

Böttcher et al., [23], proposed another approach to address the varying  $Pr_t$  by making use of look-up tables where the value of  $Pr_t$  had dependence on bulk Reynolds number and  $y^+$  values.  $Pr_t$  values across the entire domain are calculated by linear interpolation. This model gave reasonable predictions. Although this model also poses limitations due to which the results needed some improvements:

- The solver must know the  $y^+$  values.
- In case of natural and mixed convection, the thermal field is not predicted well as the buoyancy effects are not considered.

#### 4.3.5. GENERAL GRADIENT DIFFUSION HYPOTHESIS

Daly and Harlow, [24], proposed a model which was aimed at improving the accuracy of SGDH. Due to the addition of the extra term to the formulation, the accuracy of the model increased a lot when compared to the SGDH model as shown by Kenjereš et al., [25]. The General Gradient Diffusion Hypothesis (GGDH) is given by:

$$\overline{\theta u_i} = -C^\theta \frac{k}{\epsilon} \left( \overline{u_i u_j} \frac{\partial T}{\partial x_j} \right). \quad (4.12)$$

The Reynolds stress term  $\overline{u_i u_j}$  is introduced in the model to consider the effects of turbulence of the flow on turbulent heat flux production.

#### 4.3.6. WET APPROACH

Launder et al., [26], proposed another model which was based on WET (Wealth  $\equiv$  Earnings  $\times$  Time) theory. According to this analogy, it was proposed to calculate the turbulent heat fluxes by multiplying the value of

the second moment by turbulent time scale. The mathematical form of the model is as follows:

$$\overline{\theta u_i} = -C^\theta \frac{k}{\epsilon} \left( \overline{u_i u_j} \frac{\partial T}{\partial x_j} + \overline{\theta u_j} \frac{\partial U_i}{\partial x_j} \right). \quad (4.13)$$

It can be observed that the model proposed above (4.13) and GGDH model are both driven by a non-isotropic diffusion process. From the equation it can be noticed that the model is considering the velocity strain and Reynolds stress for the production of the turbulent heat fluxes although it still limits itself in considering the buoyant forces directly.

#### 4.3.7. ALGEBRAIC TURBULENT HEAT FLUX MODEL

Algebraic Turbulent Heat Flux Model (AHFM) models are essentially based on the physical significance of the sources for turbulent heat fluxes. In a broader sense, these can be classified as implicit or explicit models [13, 25, 27–29]. In the framework of present work, implicit AHFM is discussed in this section.

##### IMPLICIT AHFM

Implicit model rely heavily on solving transport equation for the turbulent heat flux term. AHFM can be closed by truncating different terms from the differential equations of second order closures, resulting in different formulations [27, 30, 31]. In coming chapters it will be discussed how well implicit AHFM have performed compared to the gradient hypothesis approaches for a range of flow regimes [22, 25, 28, 32, 33]. Temperature variance  $\theta'^2$  and dissipation  $\epsilon_\theta$  can be calculated separately by solving for their transport equations.

and it resulted in four-equation  $k - \epsilon - \overline{\theta'^2} - \epsilon_{\theta'}$  which is as follows:

$$\frac{\partial \overline{\theta'^2}}{\partial t} + u_j \frac{\partial \overline{\theta'^2}}{\partial x_j} = \frac{\partial}{\partial x_j} \left( (\kappa + \kappa_t) \frac{\partial \overline{\theta'^2}}{\partial x_j} \right) + 2P_{\theta'} - 2\epsilon_{\theta'}, \quad (4.14)$$

and

$$\begin{aligned} \frac{\partial \epsilon_{\theta'}}{\partial t} + u_j \frac{\partial \epsilon_{\theta'}}{\partial x_j} = & \frac{\partial}{\partial x_j} \left( (\kappa + \kappa_t) \frac{\partial \tilde{\epsilon}_{\theta'}}{\partial x_j} \right) + C_{\epsilon 1}^{\theta'} P_{\theta'} \frac{\tilde{\epsilon}_{\theta'}}{\theta'^2} + C_{\epsilon 3}^{\theta'} P \frac{\tilde{\epsilon}_{\theta'}}{k} \\ & - C_{\epsilon 4}^{\theta'} \frac{\tilde{\epsilon}_{\theta'}^2}{\theta'^2} - C_{\epsilon 5}^{\theta'} f_{\epsilon \theta'} \frac{\tilde{\epsilon}_{\theta'} \tilde{\epsilon}}{k} + E_{\theta'}, \end{aligned} \quad (4.15)$$

where:

$$P = -\overline{u'_i u'_j} \frac{\partial \overline{u_i}}{\partial x_j}, \quad P_{\theta'} = -\overline{u'_j \theta'} \frac{\partial \overline{T}}{\partial x_j}, \quad G = -\beta g_i \overline{u_i \theta'}, \quad E_{\theta'} = 2\rho \kappa \kappa_t \left( \frac{\partial^2 T}{\partial x_j \partial x_k} \right)^2,$$

$$\tilde{\epsilon} = \epsilon - 2\nu \left( \frac{\partial \sqrt{k}}{\partial x_k} \right)^2, \quad \tilde{\epsilon}_{\theta'} = \epsilon_{\theta'} - \kappa \left( \frac{\partial \sqrt{\theta'^2}}{\partial x_k} \right)^2,$$

$$\kappa_t = C_\Phi f_\mu \frac{k^2}{\tilde{\epsilon}}, \quad f_\mu = \exp \left[ \frac{-3.4}{\left( 1 + \frac{Re_t}{50} \right)^2} \right], \quad f_{\epsilon \theta'} = 1.$$

In alternative approach of AHFM closure, to calculate  $\epsilon_\theta$  thermal timescale to mechanical timescale ratio  $R$  is defined and it is assumed to be constant. This assumption has shown good results in many flows when compared with DNS and experimental data [28, 30, 32]. This reduces the model to three equation model where it gives similar results to the four equations model as shown by Kenjereš et al., [28].

Another approach would be to solve for finding out solutions to temperature variance and dissipation. Kenjereš et al., [28] tried approximating turbulent heat fluxes based on temperature gradient, rate of strain and buoyancy. In 2005, Kenjereš et al., [25], came up with Equation (4.16) to overcome the shortcomings of the previous model as follows and was called AHFM-2005:

$$\overline{u'_i \theta'} = -C_{t_0} \tau \left( C_{t_1} \overline{u'_i u'_j} \frac{\partial T}{\partial x_j} + C_{t_2} \overline{u'_j \theta'} \frac{\partial u_i}{\partial x_j} + C_{t_3} \beta g_i \overline{\theta'^2} \right) + C_{t_4} a_{ij} \overline{u'_j \theta'}, \quad (4.16)$$

where the term anisotropy tensor is  $a_{ij} = \frac{\overline{u'_i u'_j}}{k} - \frac{2}{3} \delta_{ij}$  and  $\delta_{ij}$  is Kronecker delta.

#### 4.3.8. AHFM-NRG

Within the framework of European Union sponsored project Thermal Hydraulics of Innovative Nuclear Systems (THINS), with goal of calibration and assessment of AHFM-2005 for low Prandtl fluids, AHFM-2005 was implemented in commercial code STAR-CCM+, [34]. Shams et al., [13], calibrated the model coefficient  $C_{t_1}$  by proposing a correlation for  $C_{t_1}$ , to have better results for selected test cases, when compared to a DNS database. Also due to the numerical stability issues,  $C_{t_4}$  was taken as 0 and the resulting model was called AHFM-NRG. This model can be described as follows:

$$\overline{u'_i \theta'} = -C_{t_0} \tau \left( C_{t_1} \overline{u'_i u'_j} \frac{\partial T}{\partial x_j} + C_{t_2} \overline{u'_j \theta'} \frac{\partial u_i}{\partial x_j} + C_{t_3} \beta g_i \overline{\theta'^2} \right) \quad (4.17)$$

#### 4.3.9. SIGNIFICANCE OF MODEL

Equation (4.17) defines a turbulent heat flux model based on :

- Turbulent heat fluxes from mean temperature gradient  $\left( \frac{\partial T}{\partial x_j} \right)$
- Turbulent heat fluxes due to a mean rate of strain  $\left( \frac{\partial u_i}{\partial x_j} \right)$
- Turbulent heat fluxes resulting from Buoyant forces  $\left( \rho g_i \overline{\theta'^2} \right)$

The first term of the model defines the production of turbulent heat fluxes from mean temperature gradient across domain and the turbulence of the flow. If we look at closely, the turbulent heat fluxes are generated in the direction perpendicular to the temperature gradient. The second term accounts for the turbulent heat flux generating due to the mean rate of velocity strain and the third term accounts for the generation of turbulent heat fluxes resulting from buoyant forces. The model coefficients define the weight of each term in overall turbulent heat flux production. Essentially, all the thermal convective flows can be broadly categorized into these categories: Forced, Natural and Mixed. For forced convection, the dependence of  $C_{t_1}$  on flow defining numbers such as Reynolds and Prandtl number, is reported by Shams et al., [13]. Similarly for  $C_{t_3}$ , its dependence on Rayleigh and Prandtl numbers is reported by Shams et.al, [22].

## 4.4. CALIBRATION

The previous work done in turbulent heat flux modeling for thermal predictions, the THF model is based on linear turbulence model  $k - \varepsilon$ . The linear closure of turbulent momentum flux term does not predict turbulence well in complex flow conditions. Due to inaccuracy in predictions of Reynolds stresses, the turbulent heat fluxes deviate from mean behavior leading to inaccurate thermal field prediction [35–38]. To overcome this, Shams et al., [39], extended this model to second order turbulent momentum flux closure model. The AHFM-NRG model was extended with RSM-EB (Reynolds Stress model Elliptic Blending) for Forced convection flow regime. This formulation was called AHFM-NRG:RSM-EB. Since the turbulence model employed in the formulation was changed, the coefficients were re-calibrated in order to accommodate the model

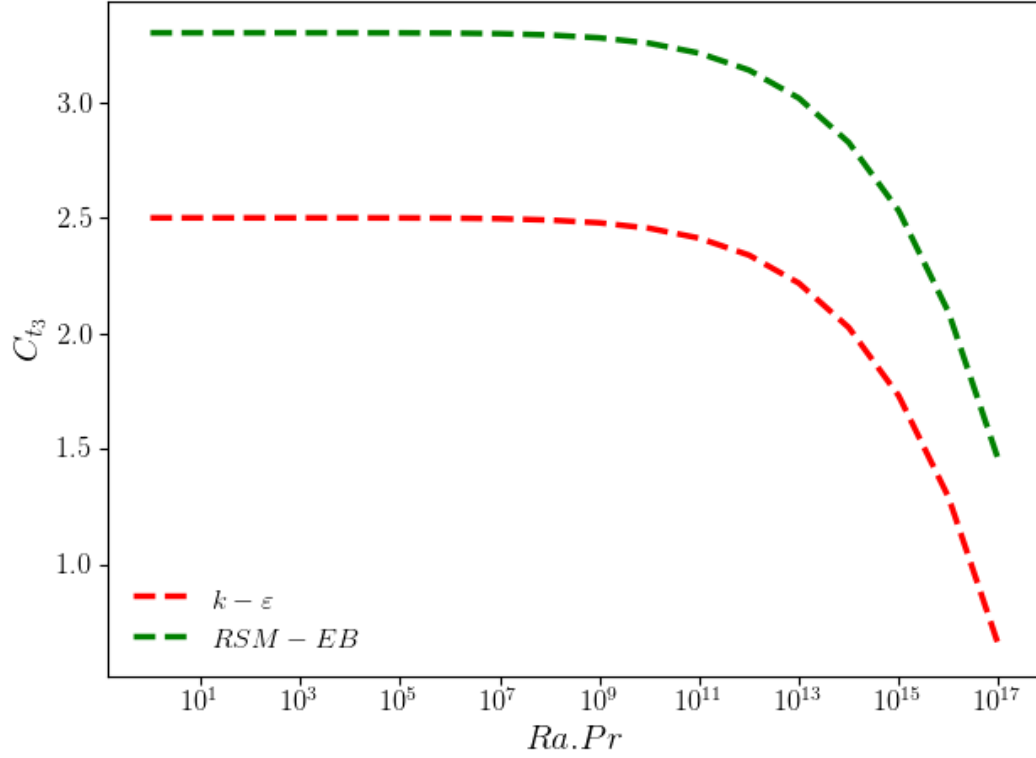


Figure 4.4: Graphical representation of  $C_{t_3}$  for AHFM-NRG: $k-\epsilon$  and AHFM-NRG+: $RSM-EB$

changes. Similarly in the framework of this thesis project, AHFM-NRG formulation is extended to natural convection flows coupled with RSM-EB. This model in the coming chapters will be referred to as AHFM-NRG+:RSM-EB. Since the governing coefficient of natural convection is  $C_{t_3}$ , it is re-calibrated for AHFM-NRG coupled with RSM-EB by considering DNS and available experimental results as reference data. In the calibration phase, Rayleigh Bénard natural convection is considered for the calibration process and different test cases were considered and results were compared with reference DNS data. Figure 4.4 describes the change in  $C_{t_3}$  correlation. The red dotted line describes  $C_{t_3}$  formulation for AHFM-NRG+: $k-\epsilon$  whereas the green dotted line describes the new correlation for AHFM-NRG+:RSM-EB. Equation 4.18 states  $C_{t_3}$  dependence on the Rayleigh number and the Prandtl number of the fluid.

$$C_{t_3} = a_1 \cdot \log^7(RaPr) + a_2 \quad \text{with} \quad 10^0 < Ra.Pr < 10^{17}. \quad (4.18)$$

In the above correlation the value of  $a_1$  is  $-4.5 \times 10^{-9}$  and  $a_2$  is 3.3 where Ra and Pr represent Rayleigh and Prandtl number of the given flow respectively.

# 5

## APPLICATION PHASE

Rayleigh Bénard natural convection (RBC) is one of the most computationally and experimentally studied cases [40–42]. It is considered to be the prototypical case for free thermal convection. In nuclear applications, passive cooling systems are integral part of the cooling process [43, 44]. To design a sustainable cooling process for reactors, it is highly important to study the heat transfer and flow of the coolant fundamentally. Owing to such high responsibility, the heat transfer and flow must be accurately predicted. The accuracy of the thermal field depends highly on the heat flux model used in numerical simulation. In a typical RBC case, a fluid layer is heated from the bottom. Expanded fluid offers buoyant forces in the domain and sets the fluid in motion. In the framework of present project, a planar geometry is considered. In coming sections, this case will be explained in detail. Also the results obtained from the simulations will be presented and discussed in this chapter.

### 5.1. COMPUTATIONAL DOMAIN

In this work, a planar rectangular geometry with constant fluid properties, will be considered for numerical simulations. Figure 5.1 describes geometry of the computational domain used. The aspect ratio of 1:8 is considered for the geometry. As shown in Figure 5.1, different layers of the domain are walls with different boundary conditions. The upper wall is maintained at lower temperature ( $T_c$ ) of 299.5 K and lower wall is maintained at higher temperature ( $T_h$ ) of 300.5 K. The wall-normal temperature difference ( $T_h - T_c$ ) of 1 K is kept constant throughout the simulations which is responsible for the buoyant forces that put the fluid in motion. The gravitational acceleration ( $g$ ) acts downward along y-axis. The fluid flow and thermal field are defined by Rayleigh number defined as  $Ra = g \beta \Delta T H^3 / (\nu \alpha)$  where  $g$  is the gravitational acceleration,  $\beta$  is the thermal expansion coefficient,  $H$  is the characteristic length,  $\Delta T$  is the constant temperature difference between the domain walls,  $\nu$  is the kinematic viscosity and  $\alpha$  is the thermal diffusivity and Prandtl number as  $Pr = \nu \rho c_p / k$  where  $\rho$  is fluid density,  $k$  is thermal conductivity and  $c_p$  is specific heat at constant pressure of the fluid.

At the top and bottom walls iso-thermal conditions i.e. Dirichlet boundary condition is imposed for thermal and no-slip boundary condition for velocity. In the stream-wise and span-wise direction the, walls are imposed with periodic boundary condition for velocity to consider the flow to be periodic in nature for these directions. Table 5.1 summarizes the boundary conditions.

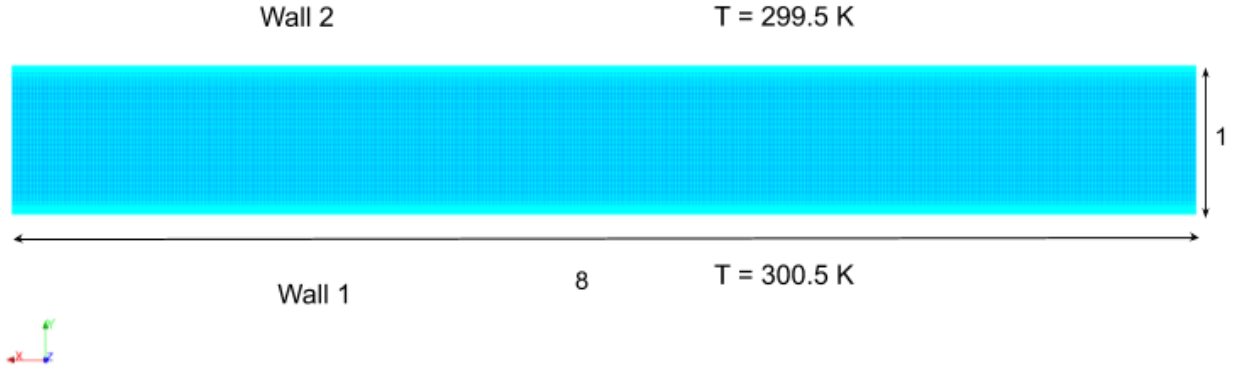


Figure 5.1: Computational domain for the RBC case

Wall	Velocity	Thermal	Remark
Bottom	No-slip	Dirichlet	$T_h = 300.5$ K
Top	No-slip	Dirichlet	$T_c = 299.5$ K
Side walls	Periodic	-	Temperature normal to wall

Table 5.1: Summary for boundary conditions imposed in the domain

## 5.2. MESH DETAILS

For the meshing of the computational domain, *SALOME* meshing platform has been used. A low Reynolds formulation of the Reynolds stress model has been used in the simulations. This requires wall refinement in the near wall region. Hence a wall-resolved mesh is necessary for stability of the solution. Mesh sensitivity analysis is done to find out the minimum number of cells required for accurate thermal and flow field predictions. The analysis is summarized in Appendix. In the present work, Mesh with 40,000 cells used. As the CFD code used for the simulations is based on finite volume method, a three dimensional domain is considered. One layer in span-wise direction is considered to minimize the computational efforts. The domain for the simulations is planar three dimensional geometry with sizes  $L_x \times L_y \times L_z = 8\delta \times 1\delta \times 0.1\delta$  where  $\delta$  is the half of width of the channel.  $y^+ < 1$  is maintained in for the mesh in CFD calculations. The  $\Delta y_{wall}$  is kept at 0.0005.

$N_x$	$N_y$	$N_z$
200	200	1

Table 5.2: Summary for mesh used in simulations

where  $N_x$  and  $N_y$  are the number of elements considered in x and y direction.

From the Figures 5.2 and 5.3 contours, Rayleigh Bénard cells can be distinctively identified by the streams of hot and cold temperature moving in the y-direction. The flow in the simulation is driven by the buoyancy effect created by the temperature difference across the domain. If we look at the contours closely, it can be seen that at the places of high temperature streams, the velocity is relatively higher in the velocity contour. In next sections, results from different cases considered in the framework of this project are presented. Important quantities to describe the thermal convection such as Mean temperature profile  $T^* = \frac{T-T_c}{T_h-T_c}$ , turbulent

kinetic energy, temperature variance and turbulent heat fluxes are compared with reference DNS data and data from simulations with other THF and TMF closures.

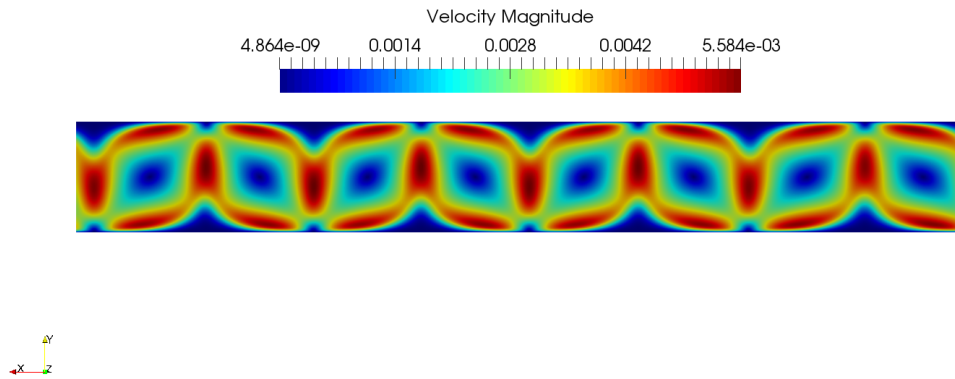


Figure 5.2: Velocity Contour for Ra 630000 Pr 0.7

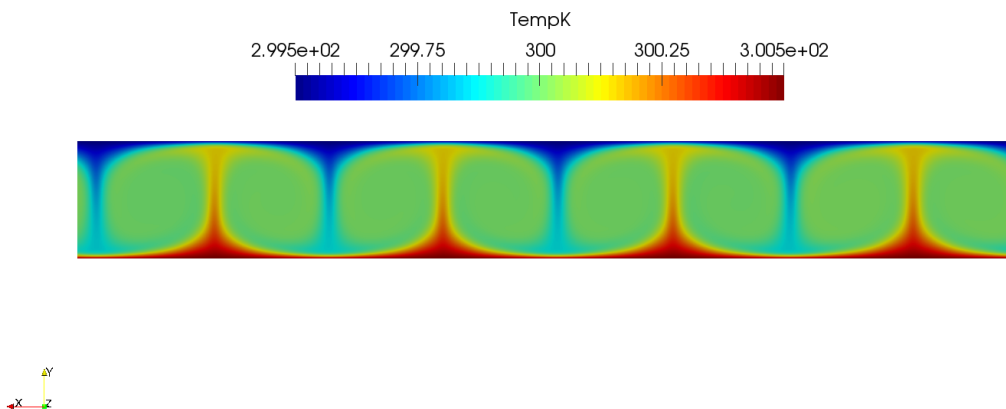


Figure 5.3: Temperature Contour for Ra 630000 Pr 0.7

### 5.3. FLOW PARAMETERS

In the case of Rayleigh Bénard natural convections, the flow is defined by Rayleigh for the flow and Prandtl number of the fluid. In the current framework of thesis project, fluids with Prandtl number 0.7 , 0.025 and 0.006 are considered. The CFD calculations aim at simulating the liquid metals used in reactors. The liquid metals have low Prandtl number i.e. relatively high thermal diffusivity compared to viscous diffusivity. A wide range of Rayleigh numbers are considered in the simulations ranging from 24000 to 20000000. As discussed in previous chapter, liquid metals are considered to be very good coolant in nuclear applications which motivates the selection of test cases with the considered Prandtl numbers. Table 5.3 gives examples for the different Prandtl fluids considered in the present work.

Pr number	Example
0.7	Air
0.025	Mercury
0.006	Molten Sodium

Table 5.3: Fluid examples for Prandtl numbers considered in the present work

## 5.4. SIMULATION SETTING

In the present work, to validate the correlation formed in the previous chapter as part of calibration of coefficient  $C_{t_3}$  for natural convection flow regimes, the following set of simulations are carried out. The results obtained from the simulation with TMF closure with RSM-EB and THF as AHFM-NRG+ are referred to as AHFM-NRG+:RSM-EB. Table 5.4 describes the nomenclature for the data presented below. The unsteady-RANS simulations with Reynolds stress model, are done with *Code\_Saturne*, [45] and RANS simulations with linear low-Re  $k - \epsilon$  model are done using commercial CFD solver STAR-CCM+, [34]. In a steady RANS calculation, for Pressure-Velocity coupling SIMPLE, Patankar et al., [46], algorithm has been used and on the other hand, for unsteady RANS calculations SIMPLEC, Doormaal et al., [47], algorithm has been used in *Code\_Saturne*. In all the calculations second order linear upwind discretization scheme is used for all the variables.

Label	TMF	THF	Code
SGDH: $k - \epsilon$	Lien low-Re $k - \epsilon$	Reynolds Analogy	STAR-CCM+
AHFM-NRG: $k - \epsilon$	Lien low-Re $k - \epsilon$	AHFM-NRG+	STAR-CCM+
SGDH:RSM-EB	RSM-EB	Reynolds Analogy	<i>Code_Saturne</i>
AHFM-NRG:RSM-EB	RSM-EB	AHFM-NRG+	<i>Code_Saturne</i>

Table 5.4: Summary of the turbulence models used in the present work

## 5.5. SELECTION OF TEST CASES

In this section, the simulation cases described in Table 5.5, will be presented and these cases will be discussed below to understand the effect of calibrated coefficient in accurately predicting the thermal field and flow for given flow parameters.

### 5.5.1. TEST CASES

In the present work, six different cases are considered to compare the performance of AHFM-NRG+:RSM-EB model with Reynolds analogy and other turbulent heat flux closures. Shams, [22] selected three cases with different Prandtl fluids for their validation analysis. Similarly on the same lines, following cases are considered as it will be easy to perform comparative study and analyze data for these cases. Also present work includes three additional cases for validation purpose. Case-1 with Ra number as  $2 \times 10^7$ , from Table 5.5 is considered to study the performance of the model at moderately high Rayleigh number. Table 5.5 summarizes the cases considered in the present work.

Test Cases	Rayleigh number	Prandtl number	Reference
Case-1	20000000	0.7	R. Kerr, [48]
Case-2	630000	0.7	Otic et al., [49]
Case-3	381000	0.7	Wörner, [50]
Case-4	100000	0.025	Otic et al., [49]
Case-5	50000	0.025	Wörner, [50]
Case-6	24000	0.006	Wörner, [50]

Table 5.5: Selected test cases of the natural convection flow regime with RBC configuration.

### 5.5.2. DNS CASE SETUP

It is important to discuss the DNS case setup to completely understand the comparative analysis done in the framework of current project. In this section, the DNS case setup performed by Wörner, [50] will be discussed.

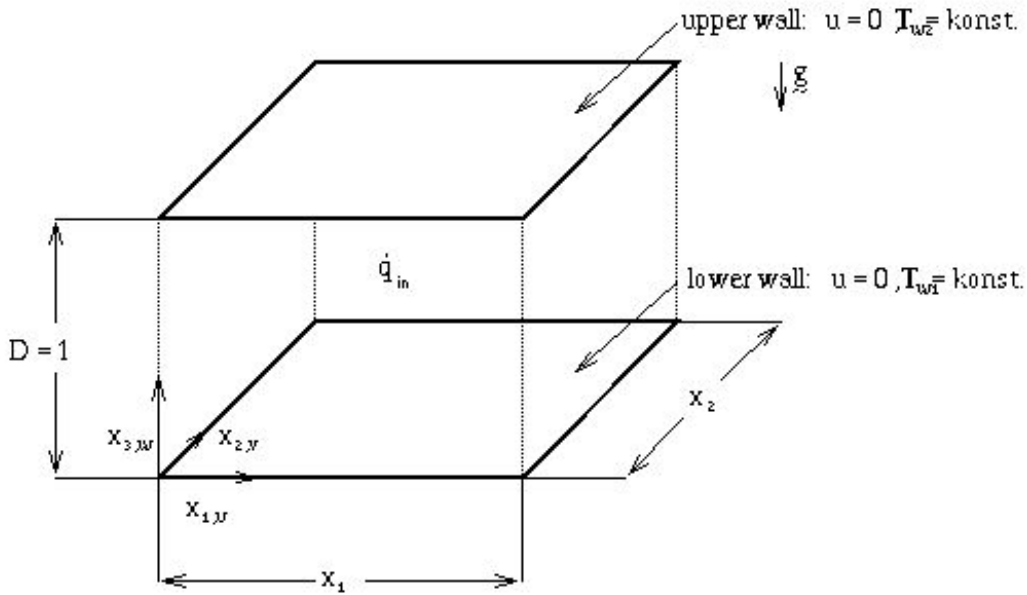


Figure 5.4: DNS case geometry with boundary conditions imposed

Figure 5.4 describes the geometry of the case considered for DNS. The aspect ratio of the domain is 1:8. The height between the two walls maintained at different temperatures is 1. The value of  $X_1$  i.e. the size of the domain along the  $x$ -axis is 8 for cases with  $Pr = 0.006$  and  $0.025$  and  $7.92$  for  $0.7$ . The value of  $X_2$  i.e. in the  $z$ -direction, is taken equal to  $X_1$ . The upper and lower wall are kept at constant temperatures and hence resulting in constant temperature gradient with slip velocity to be zero. Transient 3d direct numerical simulation code TURBIT is employed as CFD solver for calculations. Reference data from the DNS calculations suggested that the the fluctuations in the  $z$ -direction are nearly zero. Hence for optimizing the computational time in current project considering the planar geometry is justified. In next sections, the results from simulations and DNS reference data are discussed is

### 5.5.3. CASE 1

In this section the results from the numerical simulation of Case 1 have been presented. This simulation case is defined by Prandtl number as 0.7 and Rayleigh number as 20000000. The thermal diffusivity and momentum diffusivity of the fluid are of comparable order yet the thermal diffusivity is more in magnitude. The mean temperature distribution for AHFM-NRG+:RSM-EB shows very good agreement with the reference DNS data. The Reynolds analogy approaches coupled with linear  $k-\epsilon$  model as well as second-order closure RSM-EB, fail to capture the rather steep change in the temperature distribution going away from the wall, in the near-wall region. The mean temperature distribution is seen to be diffused across the domain unlike the DNS data.  $k-\epsilon$ :AHFM-NRG+ slightly deviates away from the DNS data in the region about  $y/H = 0.15$  to  $0.10$ . Observing temperature variance plot, it can be said that the AHFM-NRG+:RSM-EB model has over-predicted the magnitude of turbulent kinetic energy (TKE) whereas the AHFM-NRG+: $k-\epsilon$  model under-predicts the by huge margin when compared with DNS data. But overall, the temperature variance trend by DNS data has been closely followed by AHFM-NRG+:RSM-EB model and also have predicted the location for TKE maxima. In conclusion, for this case the AHFM-NRG+:RSM-EB has improved results by a comparable margin than THF closure of AHFM-NRG+: $k-\epsilon$  model.

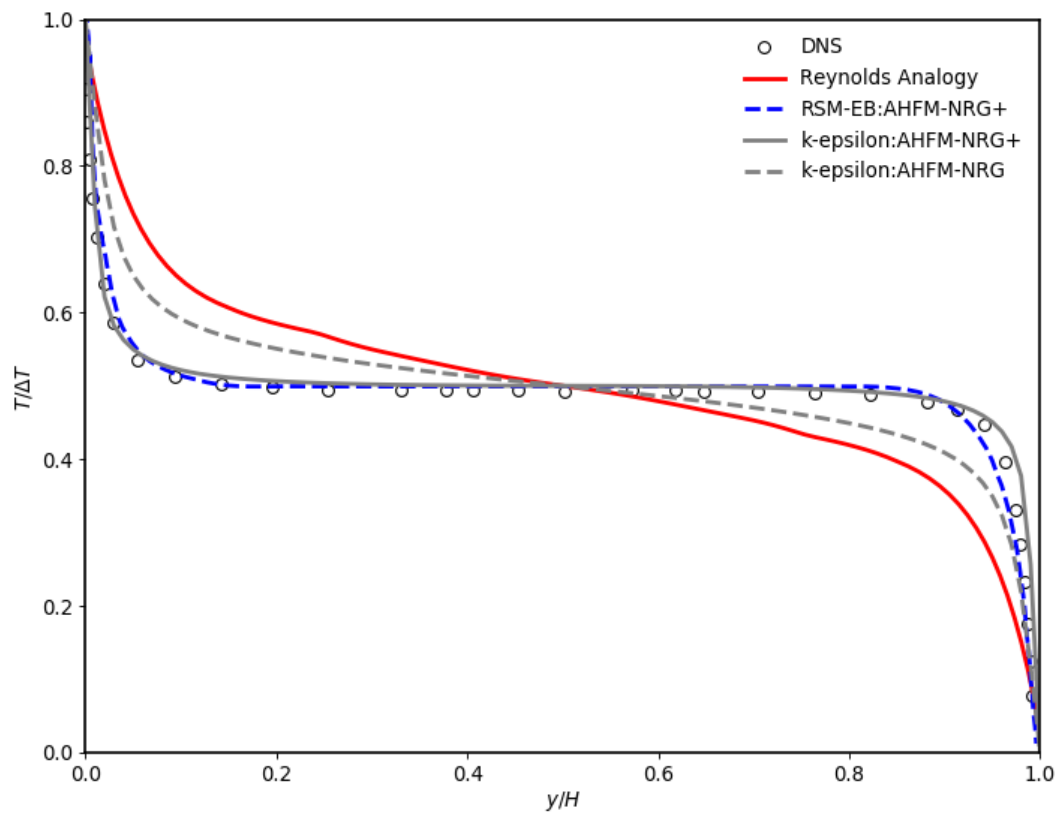


Figure 5.5: Mean temperature distribution for Ra 2e7 Pr 0.7

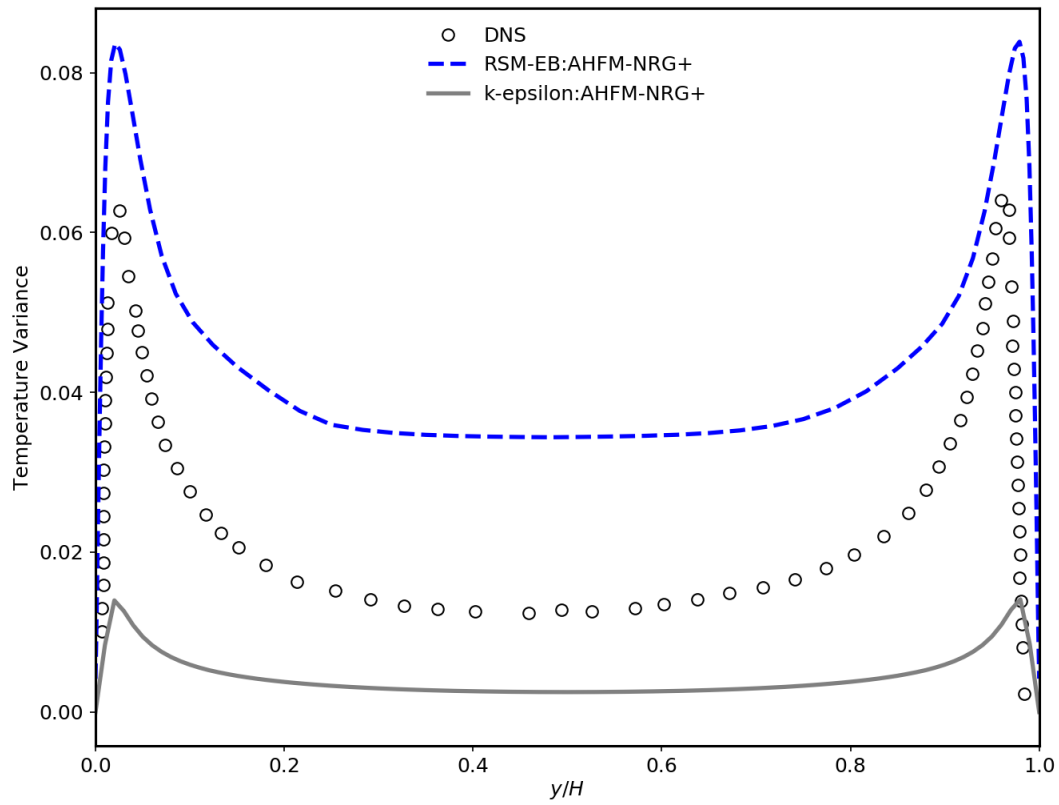


Figure 5.6: Temperature Variance for Ra 2e7 Pr 0.7

### 5.5.4. CASE 2

In this section the results from the numerical simulation of Case 2 have been presented. This simulation case is defined by Prandtl number as 0.7 and Rayleigh number as 630000. The mean temperature distribution for AHFM-NRG+:RSM-EB shows almost complete agreement with the reference DNS data. The Reynolds analogy approach fails to capture the rather steep change in the temperature distribution going away from the wall, in the near-wall region. The mean temperature distribution is seen to be diffused across the domain unlike the DNS data. AHFM-NRG+: $k-\epsilon$  slightly deviates away from the DNS data in the region about  $y/H = 0.15$  to  $0.10$ . Observing temperature variance plot, it can be said that the AHFM-NRG+:RSM-EB model has predicted the magnitude of temperature variance quite well whereas the AHFM-NRG+: $k-\epsilon$  model under-predicts the by huge margin when compared with DNS data. But overall the TKE trend by DNS data has been closely followed by AHFM-NRG+:RSM-EB model and also have predicted the location for TKE maxima. Closely observing TKE plot, it can be said that the magnitude of the kinetic energy is over-predicted as compared with reference DNS data whereas the Reynolds Analogy has under-predicted TKE. Overall trend across domain, is well followed by both models, given by DNS. In conclusion, for this case the AHFM-NRG+:RSM-EB has improved results by a comparable margin than THF closure of AHFM-NRG+: $k-\epsilon$  model as well as Reynolds analogy.

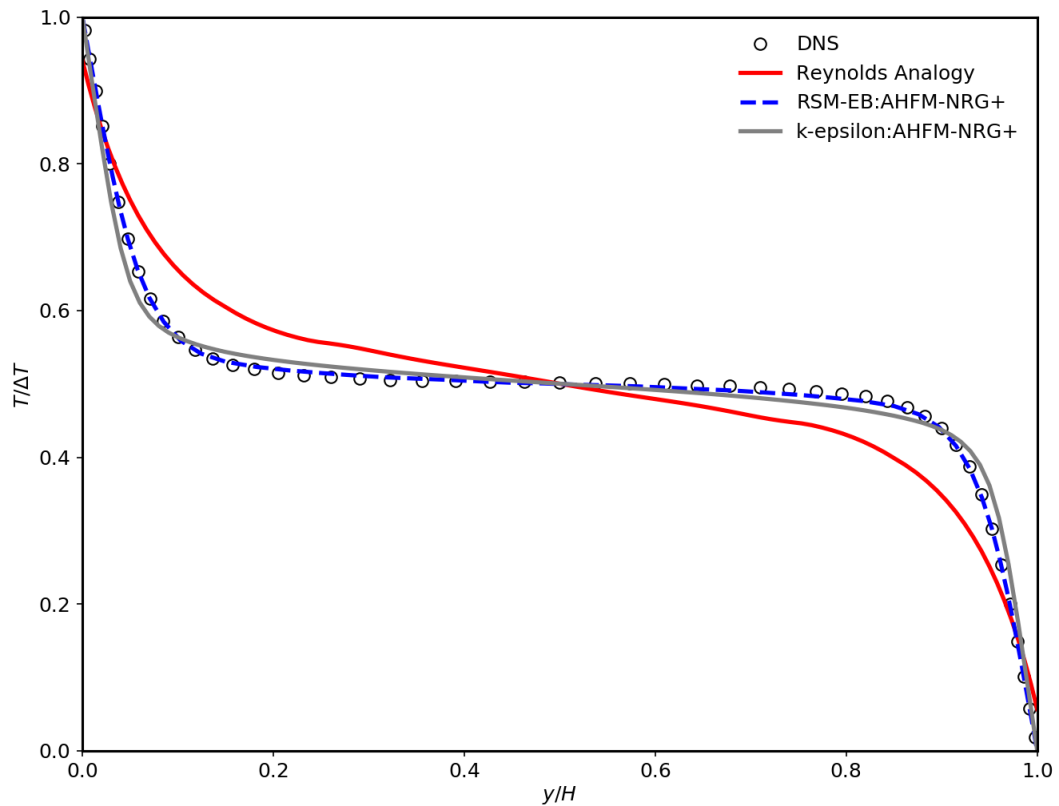


Figure 5.7: Mean temperature distribution for Ra 630000 Pr 0.7

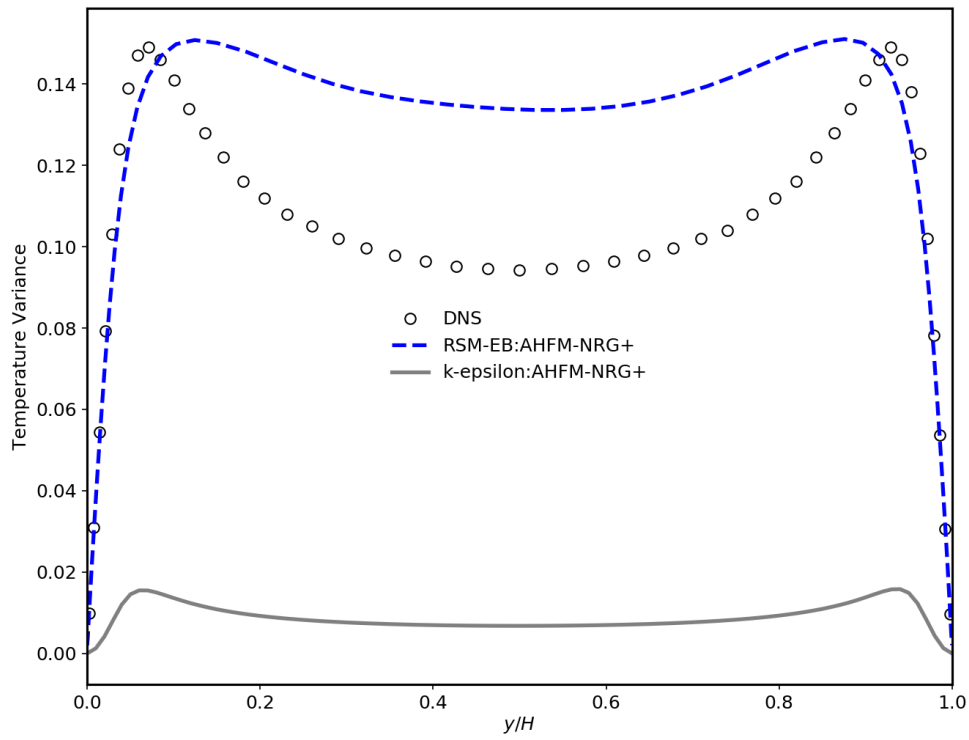


Figure 5.8: Temperature Variance for Ra 630000 Pr 0.7

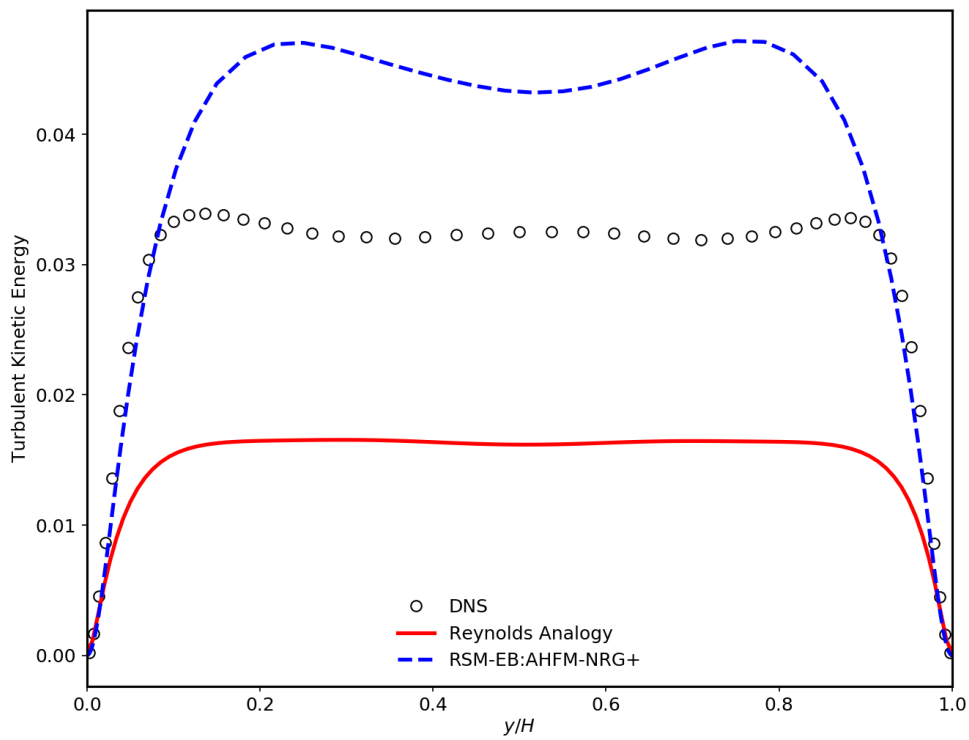


Figure 5.9: Turbulent kinetic energy for Ra 630000 Pr 0.7

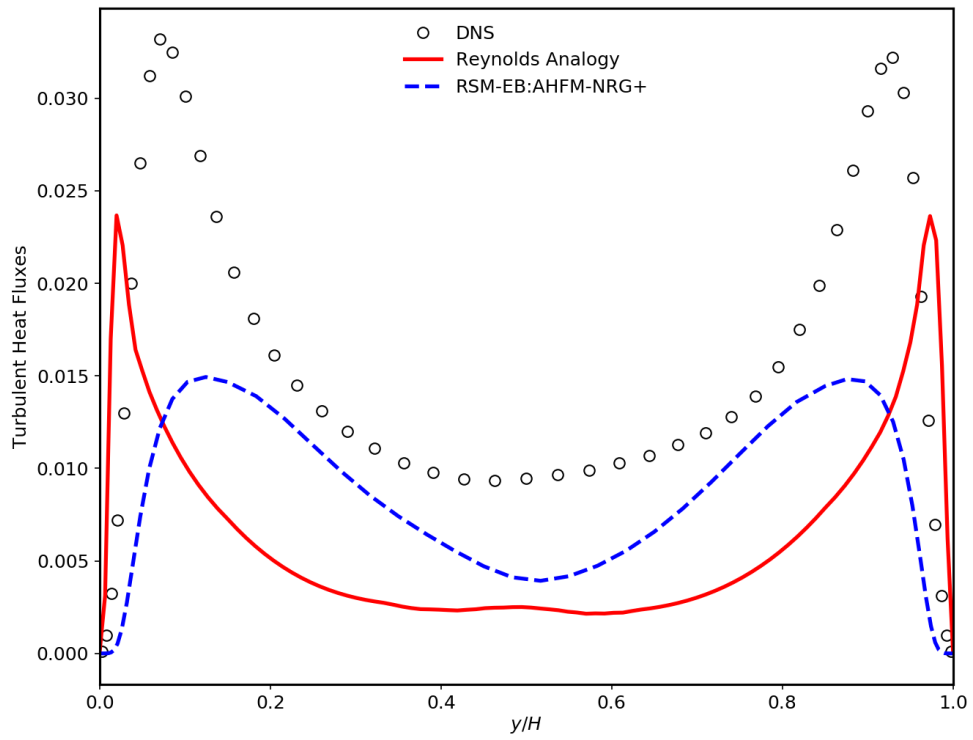


Figure 5.10: Turbulent heat fluxes for Ra 630000 Pr 0.7

### 5.5.5. CASE 3

In this section the results from the numerical simulation of Case 3 have been presented. This simulation case is defined by Prandtl number as 0.7 and Rayleigh number as 381000. The mean temperature distribution for AHFM-NRG+:RSM-EB shows excellent agreement with the reference DNS data. The Reynolds analogy approach fails to capture the temperature gradient change in the temperature distribution going away from the wall, in the near-wall region. The mean temperature distribution is seen to be diffused across the domain unlike the DNS data. AHFM-NRG+: $k-\epsilon$  slightly deviates away from the DNS data in the region about  $Y/H = 0.15$  to  $0.10$ . Observing temperature variance plot, it can be said that the AHFM-NRG+:RSM-EB model has predicted the magnitude of temperature variance quite well whereas the AHFM-NRG+: $k-\epsilon$  model under-predicts the by huge margin when compared with DNS data. But overall the TKE trend by DNS data has been closely followed by RSM-EB:AHFM-NRG+ model and also have predicted the location for TKE maxima. Closely observing TKE plot, it can be said that the magnitude of the kinetic energy is over-predicted as compared with reference DNS data whereas the Reynolds Analogy has under-predicted TKE. Overall trend across domain, is well followed by both models, given by DNS. In conclusion, for this case the AHFM-NRG+:RSM-EB has improved results by a comparable margin than THF closure of AHFM-NRG+: $k-\epsilon$  model as well as Reynolds analogy.

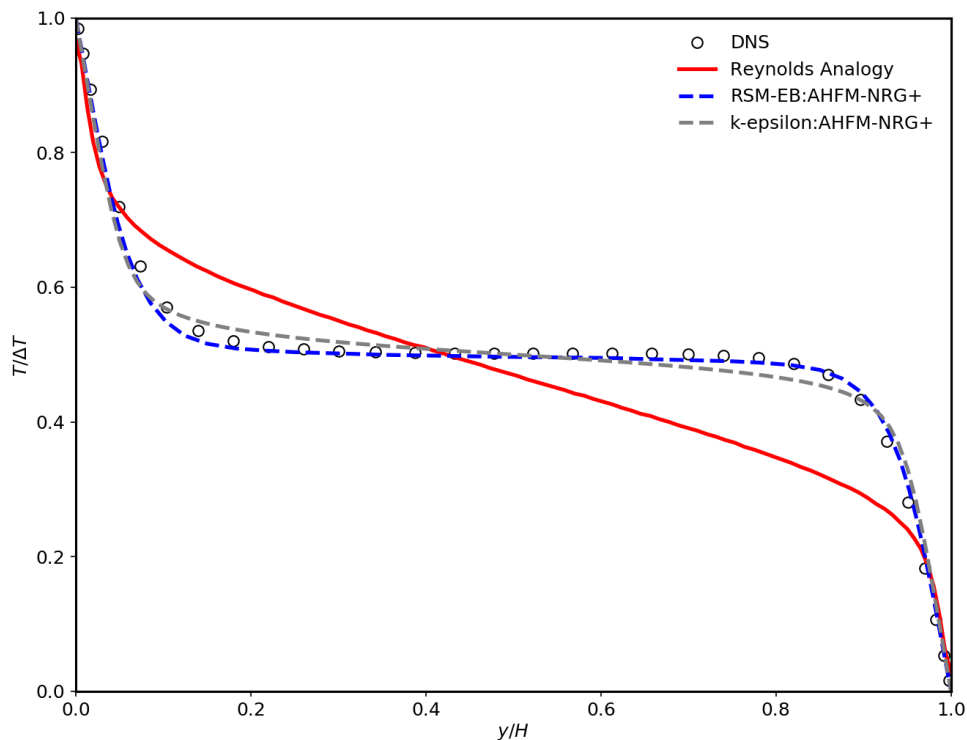


Figure 5.11: Mean temperature distribution for Ra 381e3 Pr 0.7

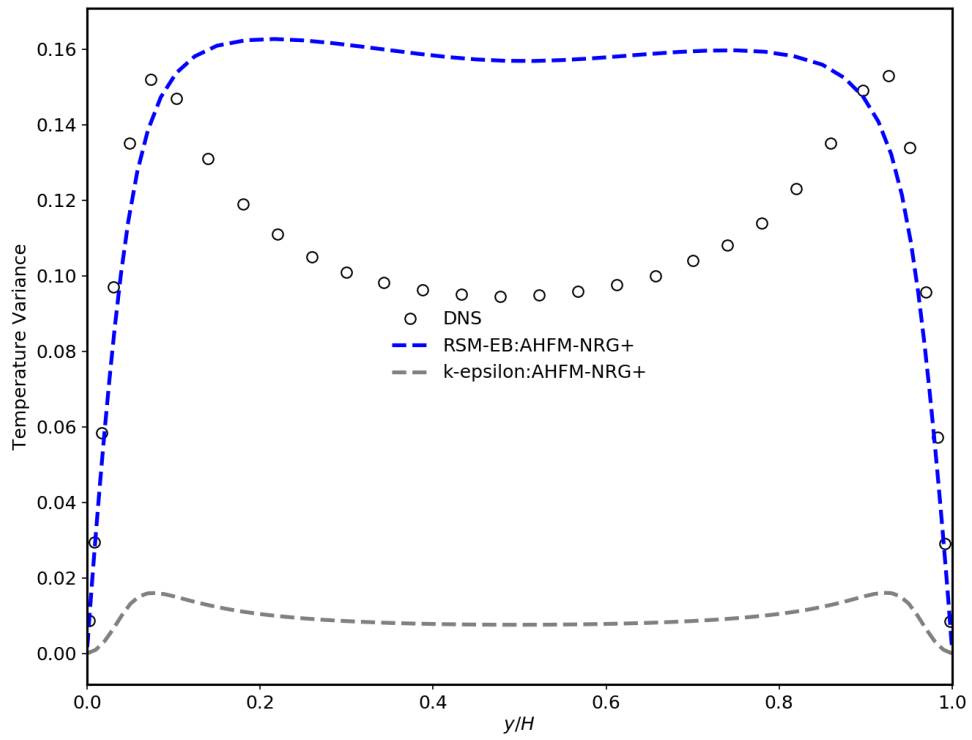


Figure 5.12: Temperature Variance for Ra 381e3 Pr 0.7

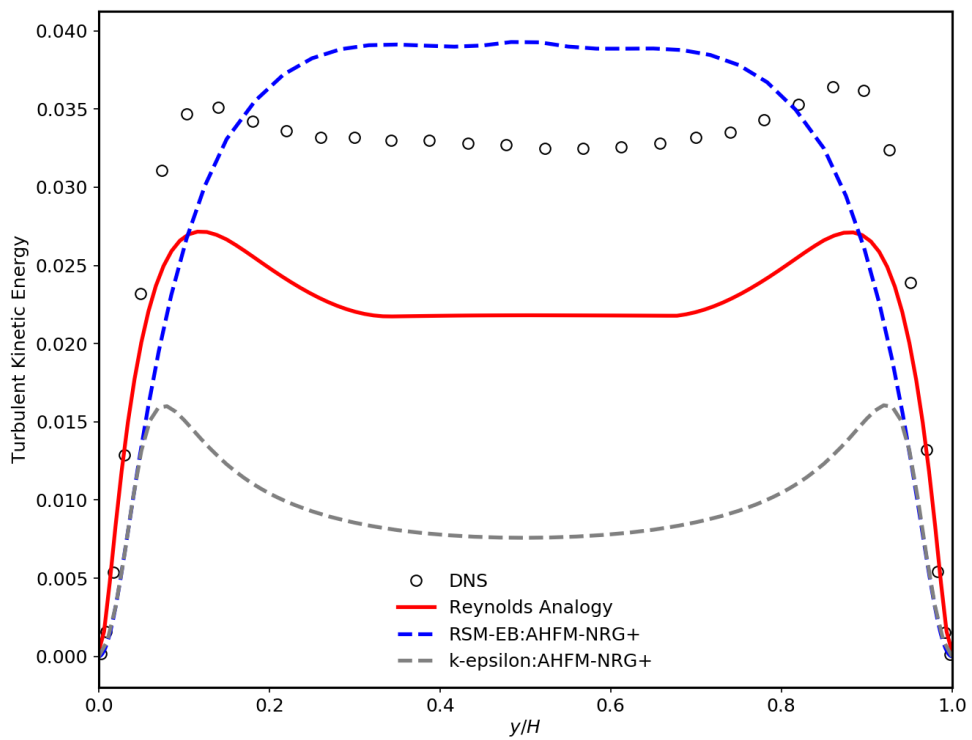


Figure 5.13: Turbulent kinetic energy for Ra 381e3 Pr 0.7

### 5.5.6. CASE 4

In this section the results from the numerical simulation of Case 4 have been presented. This simulation case is defined by Prandtl number as 0.025 and Rayleigh number as 100000. The mean temperature distribution for AHFM-NRG+:RSM-EB shows agreement with the reference DNS data. For near wall region, AHFM-NRG+:RSM-EB and AHFM-NRG+: $k-\varepsilon$  have shown slight deviation from reference data. For region  $Y/H$  0.3 to 0.7, AHFM-NRG+:RSM-EB has shown better agreement than any other THF closure. For temperature variance and turbulent kinetic energy, the AHFM-NRG+:RSM-EB model follows the trend of reference DNS data although the magnitude in both the cases has been estimated a little more. Similar trend can be seen in the case of turbulent heat flux also. The AHFM-NRG+:RSM-EB model follows the trend by DNS and gives a much better agreement with reference DNS data than Reynolds Analogy. In all the parameters AHFM-NRG+:RSM-EB has performed way better than Reynolds Analogy and temperature profile is predicted better than AHFM-NRG+: $k-\varepsilon$  model.

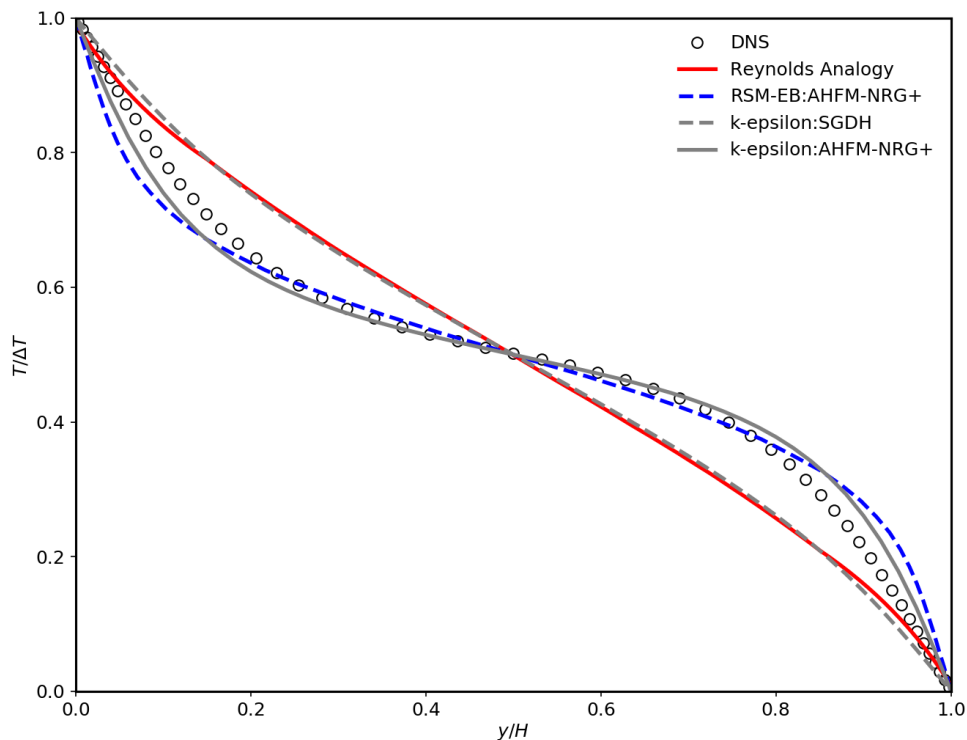
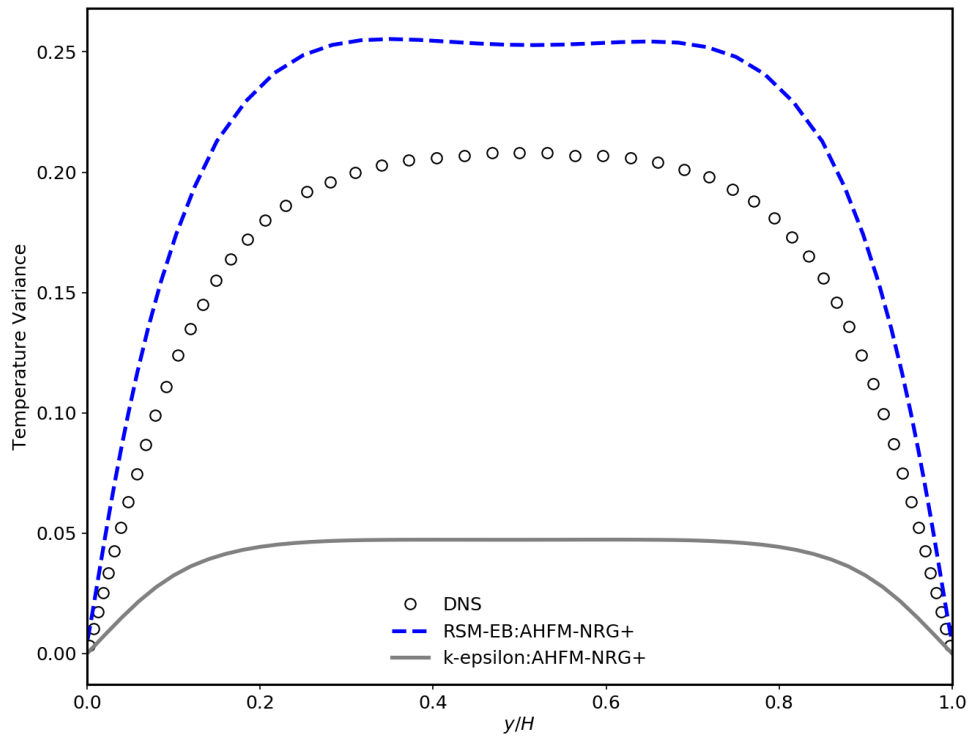
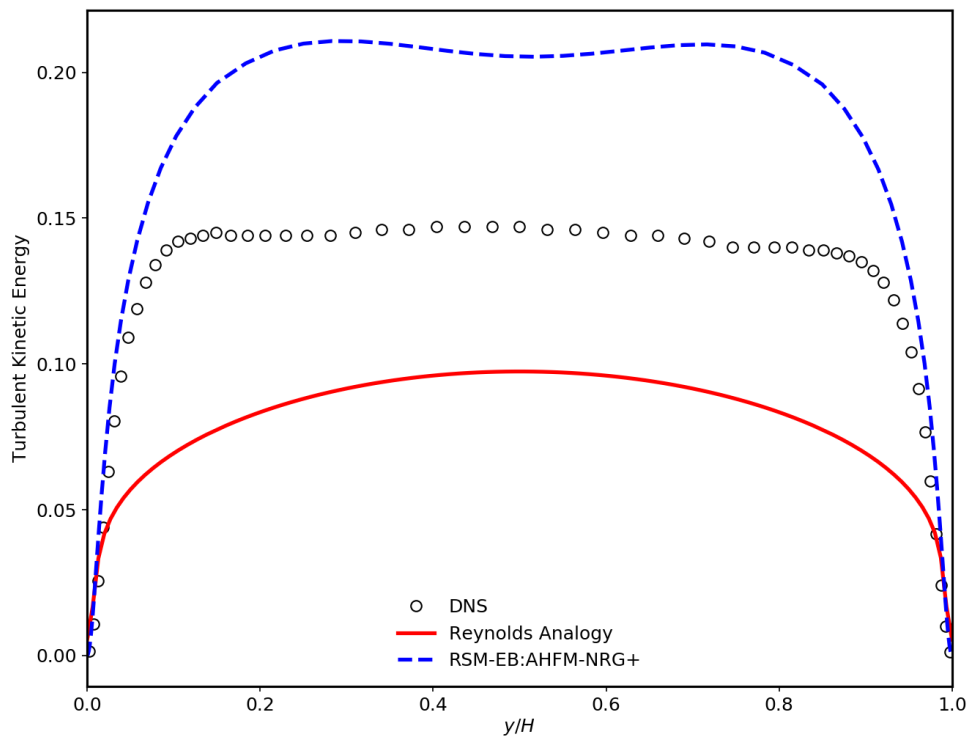


Figure 5.14: Mean temperature distribution for Ra 1e5 Pr 0.025

Figure 5.15: Temperature Variance for  $Ra = 1e5$   $Pr = 0.025$ Figure 5.16: Turbulent kinetic energy for  $Ra = 1e5$   $Pr = 0.025$

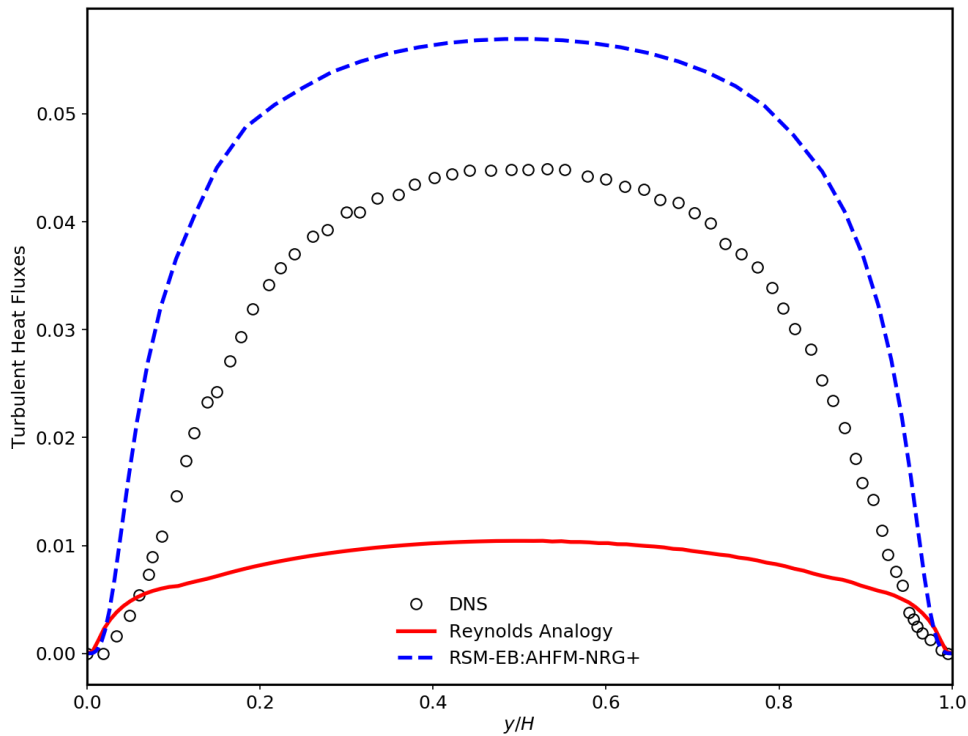


Figure 5.17: Turbulent heat fluxes for Ra 1e5 Pr 0.025

### 5.5.7. CASE 5

In this section the results from the numerical simulation of Case 5 have been presented. This simulation case is defined by Prandtl number as 0.025 and Rayleigh number as 50000. The mean temperature distribution for AHFM-NRG+:RSM-EB shows agreement with the reference DNS data. For near wall region, AHFM-NRG+:RSM-EB and AHFM-NRG+:k- $\epsilon$  have shown slight deviation from reference data. For region  $Y/H$  0.3 to 0.7, AHFM-NRG+:RSM-EB has shown better agreement than any other THF closure. For temperature variance and turbulent kinetic energy, the AHFM-NRG+:RSM-EB model follows the trend of reference DNS data although the magnitude in both the cases has been estimated a little more. Similar trend can be seen in the case of turbulent heat flux also. The AHFM-NRG+:RSM-EB model follows the trend by DNS and gives a much better agreement with reference DNS data than Reynolds Analogy. In all the parameters AHFM-NRG+:RSM-EB has performed way better than Reynolds Analogy and temperature profile is predicted better than AHFM-NRG+:k- $\epsilon$  model.

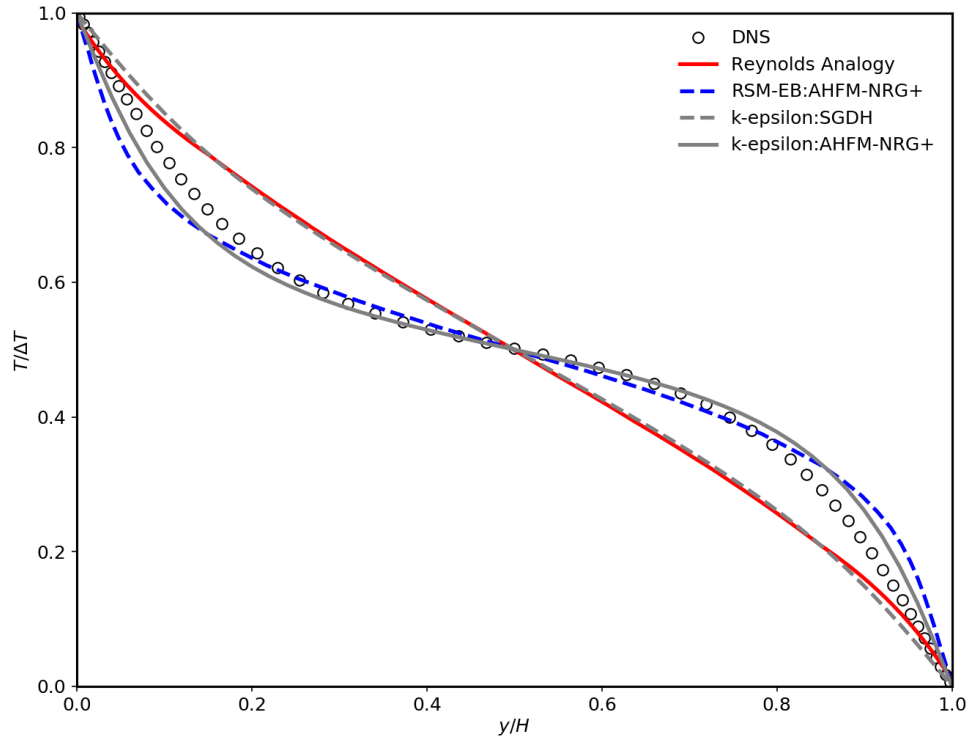


Figure 5.18: Mean temperature distribution for Ra 5e4 Pr 0.025

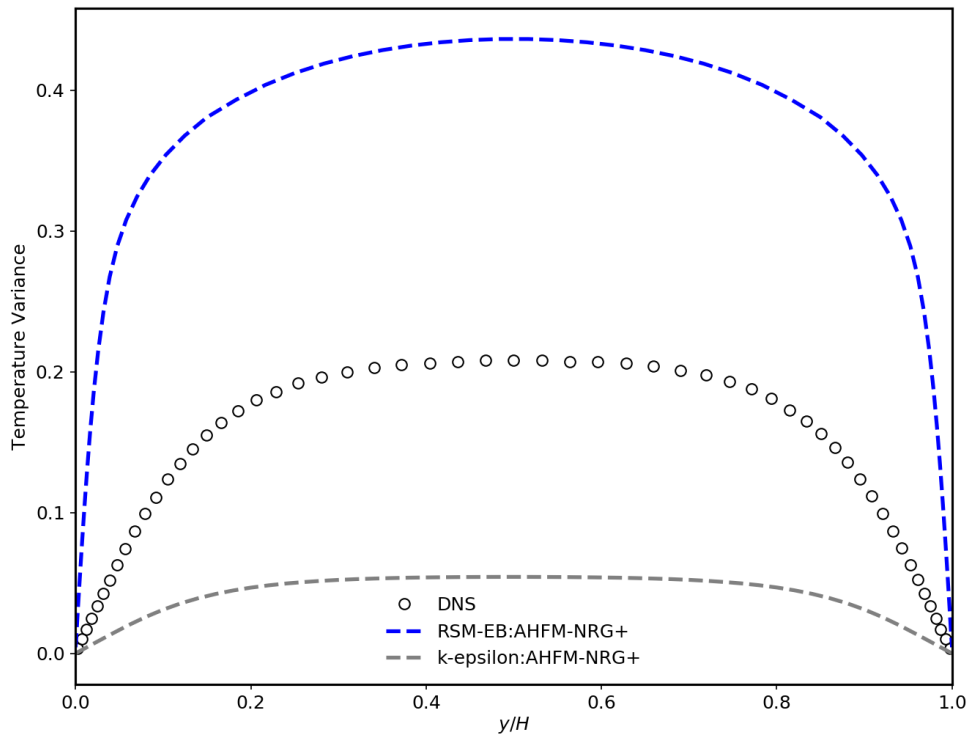


Figure 5.19: Temperature Variance for Ra 5e4 Pr 0.025

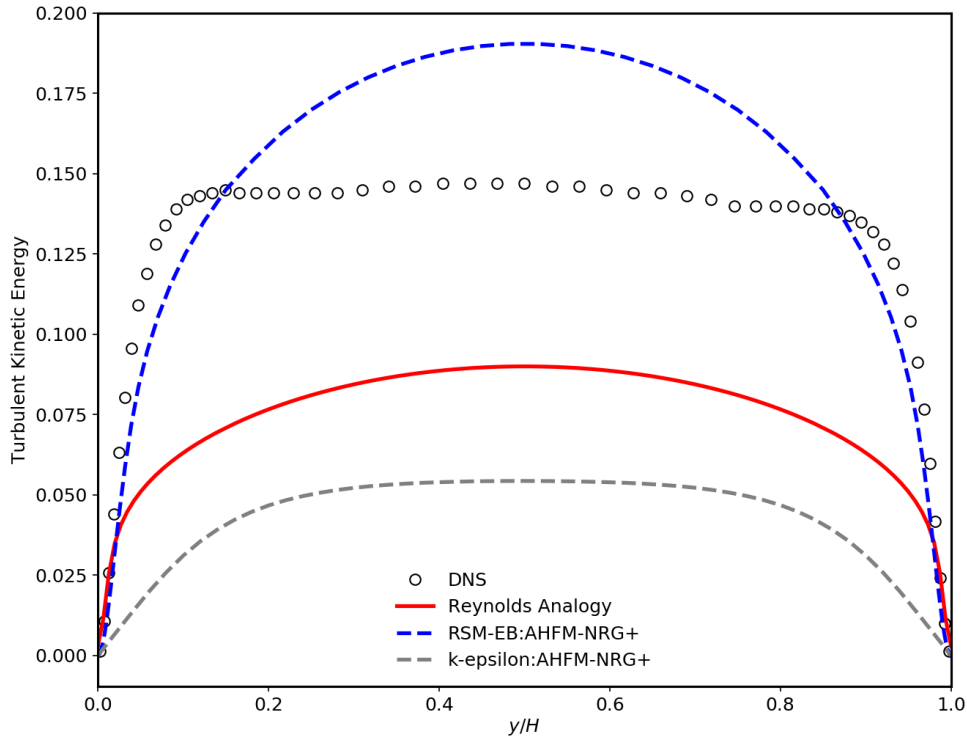


Figure 5.20: Turbulent kinetic energy for Ra 5e4 Pr 0.025

### 5.5.8. CASE 6

In this section the results from the numerical simulation of Case 6 have been presented. This simulation case is defined by Prandtl number as 0.006 and Rayleigh number as 24000. The mean temperature distribution for AHFM-NRG+:RSM-EB shows agreement with the reference DNS data. For near wall region, AHFM-NRG+:RSM-EB and AHFM-NRG+:k- $\epsilon$  have shown slight deviation from reference data. Since in this case the Pr number is very low, the fluid almost behaves like a metal and almost linear temperature profile is observed. For temperature variance, turbulent kinetic energy and turbulent heat fluxes, the AHFM-NRG+:RSM-EB model follows the trend of reference DNS data although the magnitude in this case is been underestimated. The AHFM-NRG+:RSM-EB model follows the trend by DNS and gives a much better agreement with reference DNS data than Reynolds Analogy. In all the parameters AHFM-NRG+:RSM-EB has performed way better than Reynolds Analogy and temperature profile in agreement with the AHFM-NRG+:k- $\epsilon$  model.

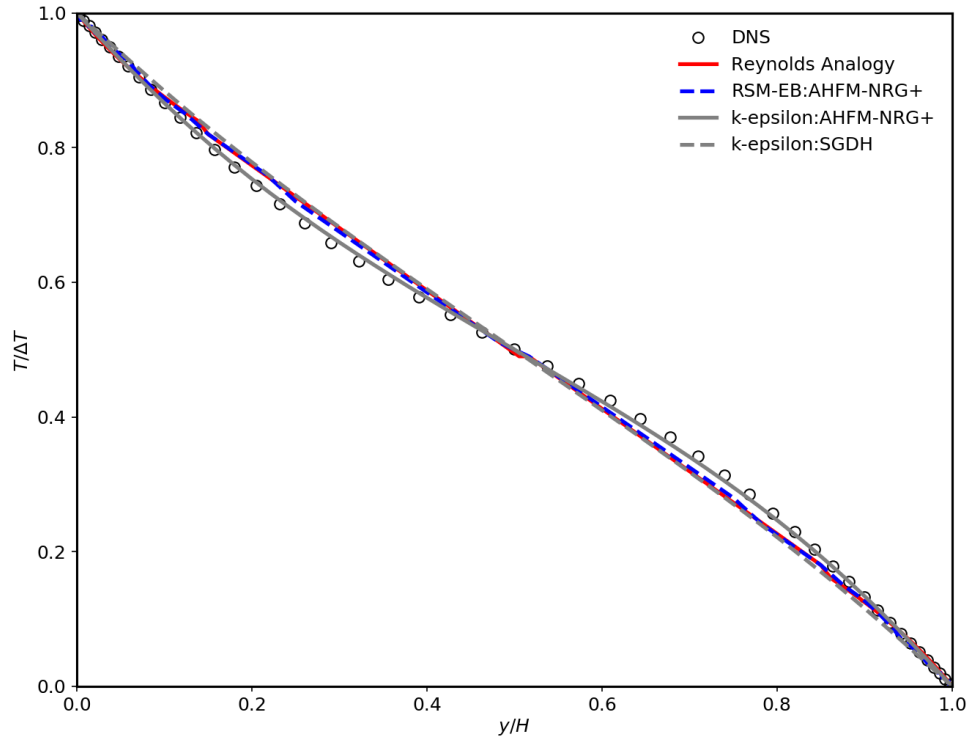


Figure 5.21: Mean temperature distribution for Ra 24e3 Pr 0.006

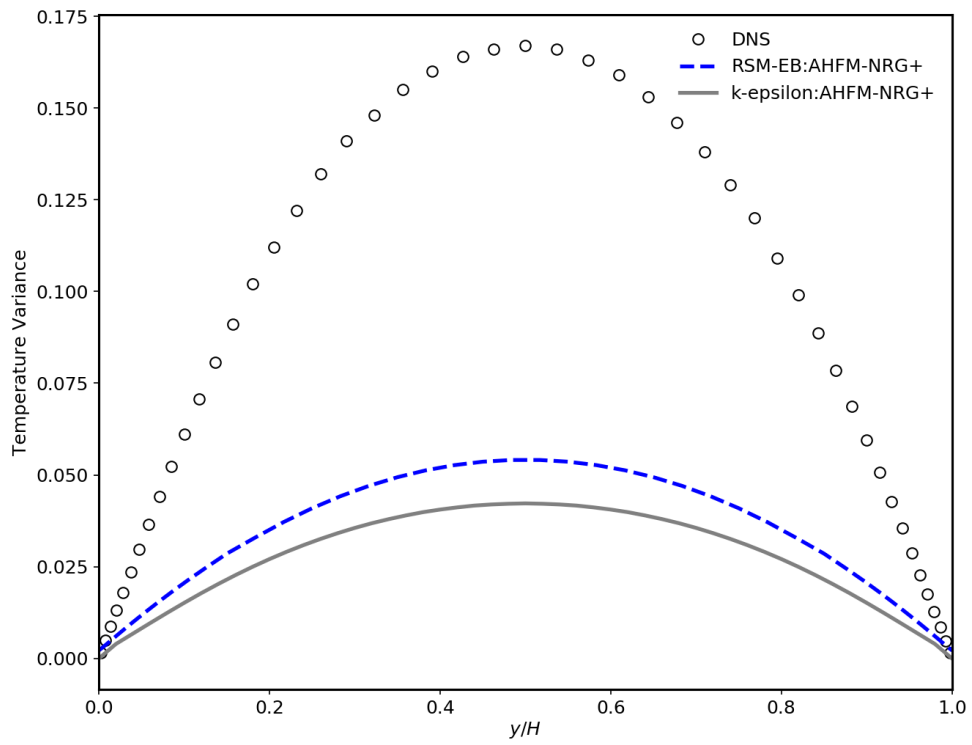


Figure 5.22: Temperature Variance for Ra 24e3 Pr 0.006

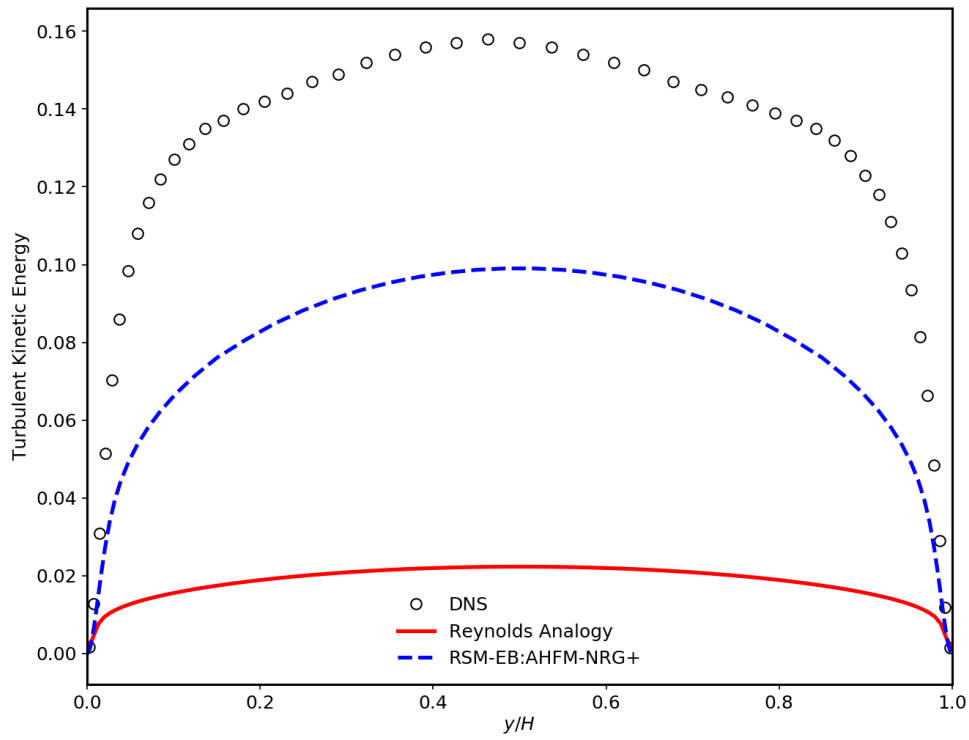


Figure 5.23: Turbulent kinetic energy for Ra 24e3 Pr 0.006

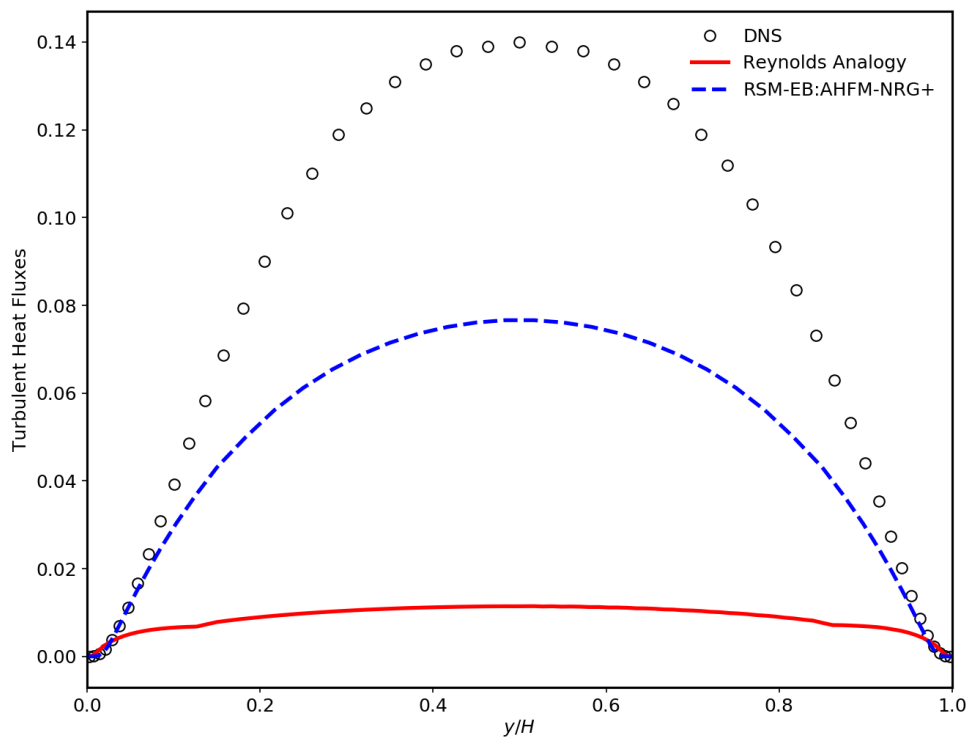


Figure 5.24: Turbulent heat fluxes for Ra 24e3 Pr 0.006



# 6

## CONCLUSION AND FUTURE SCOPE OF WORK

The primary objective of the present work is to calibrate and validate RSM-EB:AHFM-NRG+ model for turbulent heat fluxes to natural convection flow regimes and therefore the validation study has been conducted in the previous chapters. In this chapter conclusions drawn from the present work and future scope of work will be discussed.

### 6.1. CONCLUSION

Natural convection is one of the most important flow regimes for nuclear applications. The naturally driven coolant flow systems work on the principle of the natural convection. Hence it is important that the heat transfer and flow are accurately predicted. In this section, the conclusions drawn from the results of the above mentioned analysis and numerical experiment will be discussed. Focus has been given to test cases with low-Prandtl fluids as it is relevant in the nuclear applications.

- The main reason for the turbulence in the natural convection flow regimes is the buoyancy. Increase in the Rayleigh number, we observe an increase in the level of turbulence in bulk region as well as near wall. Mushroom like behavior of the flow is observed.
- As Rayleigh Bénard cells are formed, the velocity profile have seen to have periodic fluctuations representing itself in cell like structures.
- The thermal field is influenced largely by the turbulence due to buoyancy and Prandtl number of the fluid. As the Prandtl number increased from 0.025 to 0.7, the thermal field is more stable in the bulk region whereas the field shows high gradients in the near wall regions for the cases considered.
- The Reynolds analogy clearly fails to predict the thermal field accurately irrespective of the TMF model it is coupled with. This is attributed to the incomplete modeling of the turbulent heat fluxes. The limitations of this model are significantly seen as the higher Rayleigh number is achieved.
- The RSM-EB:AHFM-NRG formulation has shown some inconsistencies in predicting turbulent heat fluxes, turbulent kinetic energy and temperature variance. Although on a closer look it can be concluded that the overall mean profiles of these quantities are aligned with DNS data and considering the limitations of RANS approach, the model has performed very well.
- The calibration of the algebraic heat flux model for  $C_{t3}$  improves the thermal predictions significantly as compared to other models. Since the coefficient defines the weight of the buoyancy term in the model,

it is no surprise that we see improvements in the results due to the calibration. The results are in fair agreement with the DNS data for the respective test cases.

## 6.2. FUTURE SCOPE OF WORK

In scope of present work, AHFM-NRG+:RSM-EB model has been extended to natural convection flow regimes. For validation purposes, the prototypical case of natural convection flow regimes, i.e. Rayleigh Bénard Convection case, is chosen. Test cases with different flow properties such as Prandtl and Rayleigh number, are considered. The results from the numerical simulations are compared with reference DNS data to validate the model. The results showed excellent agreement in predicting the thermal field accurately. The AHFM-NRG+:RSM-EB model has been extended to forced convection flow regimes and has shown good improvements for industrial cases as shown by Shams et al., [39]. Since the AHFM-NRG model is calibrated and validated in natural and forced convection flow regimes, future scope of work may include validating the model for mixed convection as well. Also it will be interesting to see how coefficient  $C_{t_2}$  affects the mixed convection predictions.

Current model can be applied to cases with industrial applications, which involve natural convection flows, and experiments done in the area of natural convection regime, for understanding the behavior of the model in complex geometries and flow conditions. The test cases considered for validation study range from Rayleigh number of 24000 to 20000000. It would be very interesting to see the results from the simulations with even higher Rayleigh number such as  $10^8$  to  $10^{12}$ . The application based cases and comparative studies with experiments will help us gain the confidence in the model and also can lead us into the next step for further improvement.

Future scope may also include the automated calibration of model coefficients. The each model coefficient will be decided by the solver based on the flow conditions and fluid properties. This is an important step in moving towards a more holistic approach of numerically predicting turbulent heat fluxes in RANS methodology.

# A

## APPENDIX

### A.1. MESH SENSITIVITY ANALYSIS

In the framework of the current thesis project, calibrated model AHFM-NRG+:RSM-EB has been extended to the natural convection flows. The model validation has been conducted on a mesh that as been selected post mesh sensitivity analysis. This appendix reports the details of the mesh sensitivity analysis performed for the RANS calculations for the considered RBC setup. The mesh sensitivity analysis has been conducted for all the Prandtl numbers considered in the study which are  $Pr = 0.7$ ,  $0.025$  and  $0.006$ . In the context of reporting mesh sensitivity study, results for  $Pr = 0.7$  have been reported in the appendix. In the analysis, the THF closure has been chosen as AHFM-NRG+:RSM-EB and TMF is chosen as Reynolds stress model elliptic blending approach. The parameters describing the grids considered in the study are summarized in the following table A.1.

	Mesh 1	Mesh 2	Mesh 3
$N_x$	100	200	400
$N_y$	100	200	400
$\Delta y_{wall}$	0.001	0.0005	0.00025
$N_{total}$	10k	40k	160k

Table A.1: Summary for parameters defining the three meshes used for analysis

The refinement has been done in x and y direction. Also the  $\Delta y_{wall}$  has been maintained in such a way that the resultant mesh satisfies  $y^+ < 1$  condition for all the Prandtl numbers considered for the numerical calculations. The results obtained for mean temperature distribution, turbulent kinetic energy and temperature variance are reported below.

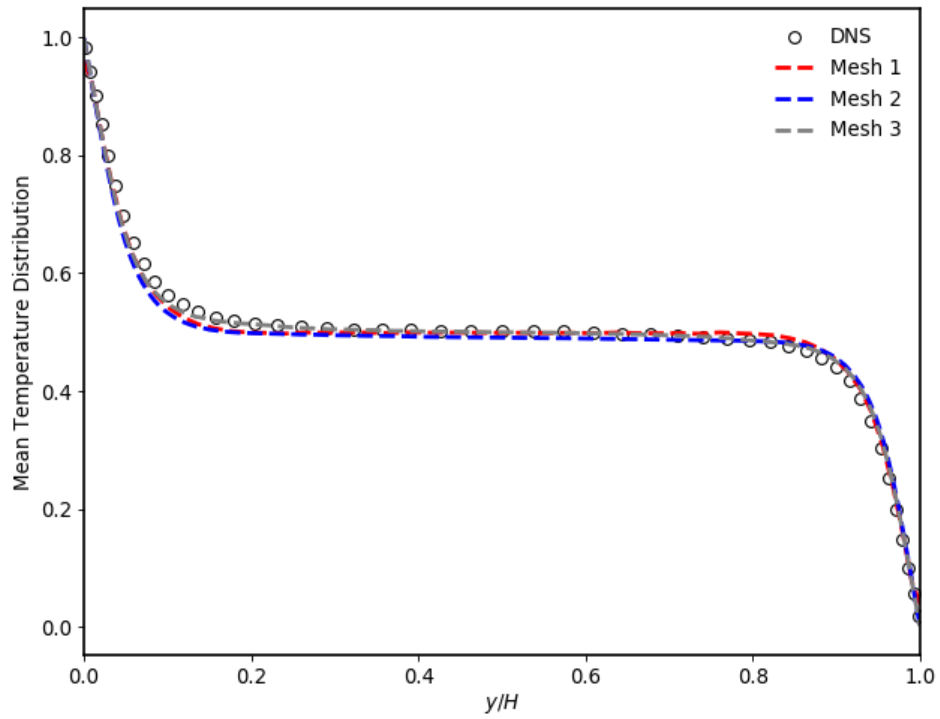


Figure A.1: Mean temperature distribution for considered three meshes

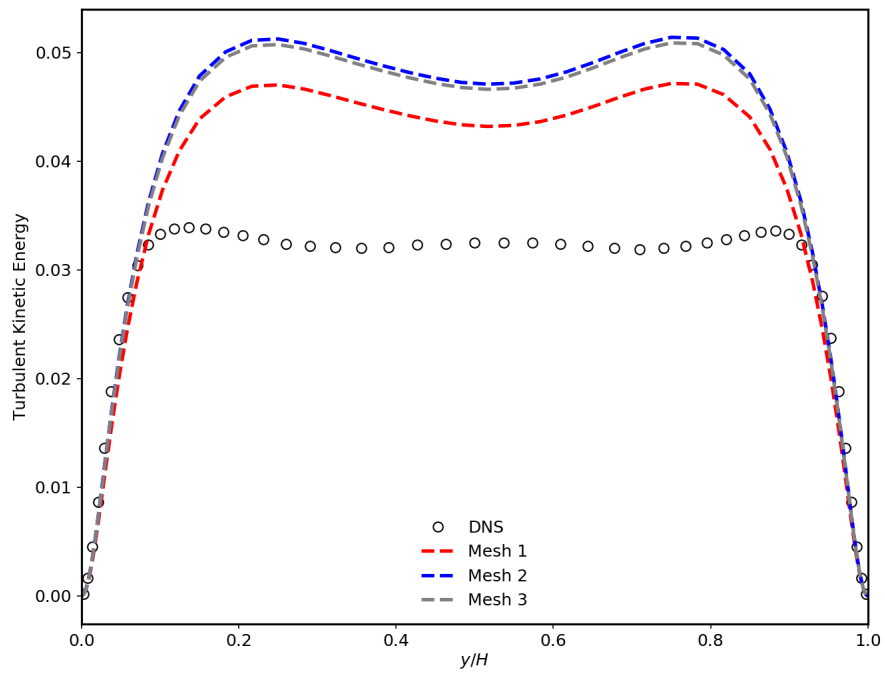


Figure A.2: Turbulent Kinetic Energy distribution for considered three meshes

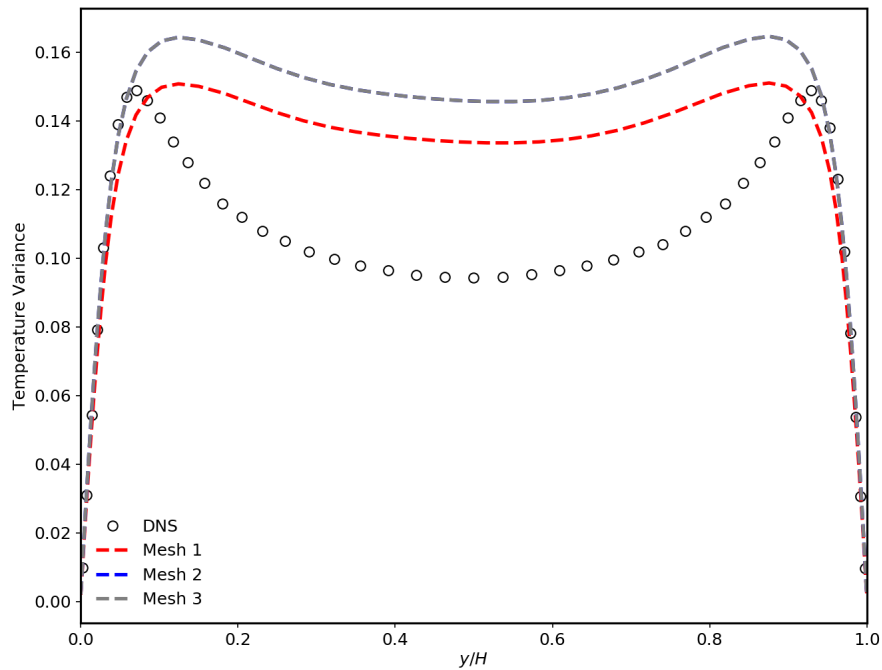


Figure A.3: Temperature variance distribution for considered three meshes

From the figures it can be seen that, the mean temperature distribution for Mesh-1 has shown slightest disagreement with DNS and Mesh-2 and Mesh-3 have shown improved results as compared with Mesh-1. Although there has not been significant improvement from Mesh-2 to Mesh-3 and the temperature profile almost follows the same plot. The deviation of Mesh-1 results for temperature distribution is as low as 0.8% with respect to Mesh-3 results. Similarly in case of temperature variance and turbulent kinetic energy, Mesh-2 and Mesh-3 have shown improvement as compared to Mesh-1. The deviation is of less than 5% for TKE and Tvar with respect to Mesh-2 and Mesh-3.

## A.2. PERTURBATIONS IN TEMPERATURE FOR Pr 0.025

This section aims at reporting perturbations observed in temperature profile for the simulations with RBC setup for fluid with Prandtl number as 0.025. It should be noticed that the perturbations are observed only for Prandtl 0.025. The perturbations although get averaged out during the averaging of the temperature profile across the entire domain. Following plot denotes the observed perturbation in temperature profile at  $x = 2.6$  along the  $y$  axis.

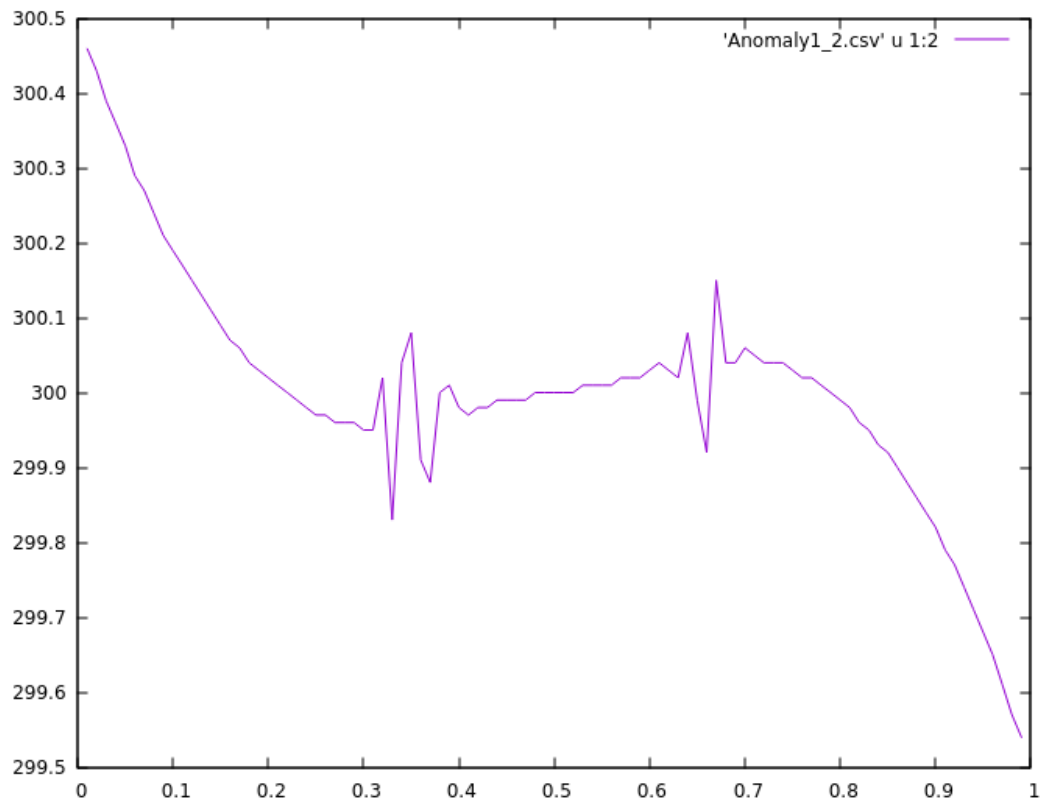


Figure A.4: Perturbations in Temperature profile

## BIBLIOGRAPHY

- [1] A. Reynolds, *The prediction of turbulent prandtl and schmidt numbers*, International Journal of heat and mass transfer **18**, 1055 (1975).
- [2] W. M. Kays, *Turbulent Prandtl number — where are we?* Journal of Heat Transfer **116**, 284 (1994).
- [3] B. Weigand, J. Ferguson, and M. Crawford, *An extended kays and crawford turbulent prandtl number model*, International journal of heat and mass transfer **40**, 4191 (1997).
- [4] M. Duponcheel, L. Bricteux, M. Manconi, G. Winckelmans, and Y. Bartosiewicz, *Assessment of RANS and improved near-wall modeling for forced convection at low Prandtl numbers based on LES up to  $Re_t=2000$* , International Journal of Heat and Mass Transfer **75**, 470 (2014).
- [5] F. Roelofs, A. Shams, I. Otic, M. Böttcher, M. Duponcheel, Y. Bartosiewicz, D. Lakehal, E. Baglietto, S. Lardeau, and X. Cheng, *Status and perspective of turbulence heat transfer modelling for the industrial application of liquid metal flows*, Nuclear Engineering and Design **290**, 99 (2015).
- [6] S. Lardeau and R. Manceau, *Computation of canonical and complex flow configurations using a robust formulation of the elliptic-blending reynolds stress model*, in *10th International ERCOFTAC symposium on Engineering Turbulence Modelling and Measurements, Marbella, Spain* (2014).
- [7] T. F. Stocker, D. Qin, G.-K. Plattner, M. Tignor, S. K. Allen, J. Boschung, A. Nauels, Y. Xia, V. Bex, P. M. Midgley, *et al.*, *Climate change 2013: The physical science basis*, (2013).
- [8] M. Delmotte, P. Zhai, H. Pörtner, D. Roberts, J. Skea, P. Shukla, A. Pirani, W. Moufouma-Okia, C. Péan, R. Pidcock, S. Connors, J. Matthews, Y. Chen, X. Zhou, M. Gomis, E. Lonnoy, T. Maycock, M. Tignor, and T. Waterfield, *Global warming of 1.5°C. an ipcc special report on the impacts of global warming of 1.5°C above pre-industrial levels and related global greenhouse gas emission pathways, in the context of strengthening the global response to the threat of climate change, sustainable development, and efforts to eradicate poverty*, (2018).
- [9] N. Energy, *Nuclear energy and kyoto protocol*, (2002).
- [10] GIF, *Introduction to Generation IV nuclear energy system and the international forum*. <http://www.gen-4.org> (2010).
- [11] S. B. Pope, *Turbulent flows*, (2001).
- [12] A. De Santis and A. Shams, *Application of an algebraic turbulent heat flux model to a backward facing step flow at low Prandtl number*, Annals of Nuclear Energy **117**, 32 (2018).
- [13] A. Shams, F. Roelofs, E. Baglietto, S. Lardeau, and S. Kenjeres, *Assessment and calibration of an algebraic turbulent heat flux model for low-Prandtl fluids*, International Journal of Heat and Mass Transfer **79**, 589 (2014).
- [14] C. Navier, *Mem acad*, R. sci. paris **6**, 389 (1823).
- [15] G. Stokes, *Sound attenuation due to viscosity*, Trans. Camb. Phil. Soc **8**, 75 (1845).

- [16] J. Boussinesq, *Theorie analytique de la chaleur vol 2 (paris: Gauthier-villars)*, (1903).
- [17] F. S. Lien, W. L. Chen, and M. A. Leschziner, *Low-Reynolds number eddy-viscosity modelling based on non-linear stress-strain/vorticity relations*, Engineering Turbulence Modelling and Experiments , 91 (1996).
- [18] B. E. Launder and B. Sharma, *Application of the energy-dissipation model of turbulence to the calculation of flow near a spinning disc*, Letters in heat and mass transfer **1**, 131 (1974).
- [19] C. J. Yap, *Modelling convective heat transfer in recirculating and impinging flows, year = 1987*, Ph.D. thesis, University of Manchester, UK.
- [20] R. Manceau and K. Hanjalić, *Elliptic blending model: A new near-wall reynolds-stress turbulence closure*, Physics of Fluids **14**, 744 (2002).
- [21] G. Ahlers, S. Grossmann, and D. Lohse, *Heat transfer and large scale dynamics in turbulent rayleigh-benard convection*, Reviews of modern physics **81**, 503 (2009).
- [22] A. Shams, *Towards the accurate numerical prediction of thermal hydraulic phenomena in corium pools*, Annals of Nuclear Energy **117**, 234 (2018).
- [23] M. Böttcher, *Cfd investigation of lbe rod bundle flow*, (2013).
- [24] F. H. B. Daly, *Transport equations in turbulence*, Physics of Fluids , 2634 – 2649 (1970).
- [25] S. Kenjereš, S. Gunarjo, and K. Hanjalić, *Contribution to elliptic relaxation modelling of turbulent natural and mixed convection*, International Journal of Heat and Fluid Flow **26**, 569 (2005).
- [26] B. Launder, *An introduction to single-point closure methodology, an introduction to the modelling of turbulence*, Lecture Series (1986-1987).
- [27] K. Hanjalić, *One-point closure models for buoyancy-driven turbulent flows*, Annual Review of Fluid Mechanics **34**, 321 (2002).
- [28] S. Kenjereš and K. Hanjalić, *Convective rolls and heat transfer in finite-length Rayleigh-Bénard convection: a two-dimensional numerical study*, Physical Review E **62**, 7987 (2000).
- [29] S. Manservigi and F. Menghini, *Triangular rod bundle simulations of a CFD  $k - \epsilon - k_\theta - \epsilon_\theta$  heat transfer turbulence model for heavy liquid metals*, Nuclear Engineering and Design **273**, 251 (2014).
- [30] H. Dol, K. Hanjalic, and S. Kenjeres, *A comparative assessment of the second-moment differential and algebraic models in turbulent natural convection*, International journal of heat and fluid flow **18**, 4 (1997).
- [31] M. Gibson and B. Launder, *Ground effects on pressure fluctuations in the atmospheric boundary layer*, Journal of Fluid Mechanics **86**, 491 (1978).
- [32] K. Hanjalić, S. Kenjereš, and F. Durst, *Natural convection in partitioned two-dimensional enclosures at higher Rayleigh numbers*, International Journal of Heat and Mass Transfer **39**, 1407 (1996).
- [33] T. Peeters and R. Henkes, *The reynolds-stress model of turbulence applied to the natural-convection boundary layer along a heated vertical plate*, International journal of heat and mass transfer **35**, 403 (1992).
- [34] SIEMENS PLM Software, *STAR-CCM+ User Guide - Version 11.06*, (2016).

- [35] E. Baglietto and H. Ninokata, *A turbulence model study for simulating flow inside tight lattice rod bundles*, Nuclear Engineering and Design **235**, 773 (2005).
- [36] L. Meyer, *From discovery to recognition of periodic large scale vortices in rod bundles as source of natural mixing between subchannels - a review*, Nuclear Engineering and Design **240**, 1575 (2010).
- [37] B. Mikuz and A. Shams, *Assessment of rans models for flow in a loosely spaced bare rod bundle with heat transfer in low prandtl number fluid*, Annals of Nuclear Energy **124**, 441 (2018).
- [38] F. Roelofs, D. Dovizio, H. Uitslag-Doolaard, B. Mikuz, and A. Shams, *Validation of wire-wrapped field assembly cfd simulations*, in *Advances in Thermal Hydraulics (ATH 2018)*, ANS Winter Meeting Embedded Topical, November, Orlando, FL (2018).
- [39] A. Shams and A. De Santis, *Towards the accurate prediction of the turbulent flow and heat transfer in low-prandtl fluids*, International Journal of Heat and Mass Transfer **130**, 290 (2019).
- [40] I. Otic and G. Grotzbach, *Statistical analysis of turbulent natural convection in low prandtl number fluids*, in *Progress in Turbulence* (Springer, 2005) pp. 203–206.
- [41] G. Grotzbach, *Direct numerical simulation of laminar and turbulent benard convection*, Journal of Fluid Mechanics **119**, 27 (1982).
- [42] G. Silano, K. Sreenivasan, and R. Verzicco, *Numerical simulations of rayleigh-benard convection for pr numbers between 10-1 and 10 4 and rayleigh numbers between 10 5 and 10 9*, Journal of fluid mechanics **662**, 409 (2010).
- [43] P. Juhn, J. Kupitz, J. Cleveland, B. Cho, and R. Lyon, *Iaea activities on passive safety systems and overview of international development*, Nuclear Engineering and Design **201**, 41 (2000).
- [44] X. Zejun, Z. Wenbin, Z. Hua, C. Bingde, Z. Guifang, and J. Dounan, *Experimental research progress on passive safety systems of chinese advanced pwr*, Nuclear Engineering and Design **225**, 305 (2003).
- [45] EDF R&D, *Code\_Saturne version 4.0.0 practical user's guide*, (2015).
- [46] S. V. Patankar and D. B. Spalding, *A calculation procedure for heat, mass and momentum transfer in three-dimensional parabolic flows*, International Journal of Heat and Mass Transfer **15**, 1787 (1972).
- [47] J. Van Doormaal and G. Raithby, *Enhancements of the simple method for predicting incompressible fluid flows*, Numerical heat transfer **7**, 147 (1984).
- [48] R. M. Kerr, *Rayleigh number scaling in numerical convection*, Journal of Fluid Mechanics **310**, 139 (1996).
- [49] I. Otić, G. Grötzbach, and M. Wörner, *Analysis and modelling of the temperature variance equation in turbulent natural convection for low-prandtl-number fluids*, Journal of Fluid Mechanics **525**, 237 (2005).
- [50] M. Worner, *Direkte Simulation turbulenter Rayleigh-Benard-Konvektion in flüssigem Natrium*, Ph.D. thesis, Kernforschungszentrum (1994).